Galaxy evolution in extreme environments

Samhitha Vadlamani

Lund Observatory
Lund University

2019-EXA149

Degree project of 60 higher education credits (for a degree of Master)
May 2019

Supervisor: Florent Renaud

Lund Observatory
Box 43
SE-221 00 Lund
Sweden

Populärvetenskaplig

Galaxies are some of the most puzzling objects in the Universe. How they form and evolve are some of the fascinating topics under investigation in the astrophysical community. Galaxies are observed to rarely evolve in isolation and a majority of them are found to be residing in groups and clusters. So, the gravitational attractions between them will drive them to interact with one another during their lifetimes. The Universe being much denser in the past (i.e higher redshifts), these interactions would have been even more frequent and hence interactions are considered important drivers of galaxy evolution. And probing the underlying physical processes during these galaxy interactions can provide insightful into understanding the galaxy evolution. Among the processes, star formation in particular is important as it determines major galactic properties such as luminosity, color, metallicity etc, and galaxy interactions trigger intense episodes of star formation in them commonly termed as 'starbursts'. Numerical models have revealed a different starburst scenario in galaxy interactions at higher redshifts in comparison with the starburst scenario at lower redshifts. Another way to attain similar initial conditions as in high redshift galaxies is through repeated encounters of galaxies at low redshifts. Extreme environments like the compact galaxy groups in the Universe are ideal locations hosting such repeated galaxy interactions. I therefore numerically model various compact galaxy group configurations corresponding to low redshifts and notice that the starburst scenarios in all our configurations are similar to one another but are different from what the other models of high redshift galaxy encounters have found. This indicates that mechanism through which similar initial conditions in interacting gaalxies are attained (i.e inherent high star formation in high redshift galaxies or star formation enhanced through repeated encounters of low redshift galaxies) dictates the situation for the evolution of star formation due to different evolutions of the factors contributing to these starbursts themselves.

Acknowledgements

I would firstly like to extend my deepest gratitude to my supervisor Florent Renaud, whose unwavering guidance, insights and feedback have been invaluable for me in not only growing academically but also as a researcher. In addition, I am grateful to my examiner Melvyn B Davies and the committee member Gregor Traven for their constructive comments and feedback in refining the thesis.

I would also like to appreciate my friends for being supportive throughout this journey and special thanks to my office-mate Loke for all the helpful discussions and to my friend Shouri for believing in my abilities and being patient to get me through my anxious and stressful moments during the Thesis. I would also like to thank my parents and family, whose love and faith have been with me in whatever I wished to pursue.

Lastly but not leastly, I express my sincere appreciation to those whom I might have forgotten to mention here but have contributed to this thesis either directly or indirectly for without any of them, this work would not have been possible.

ABSTRACT

Interactions play a crucial role in determining how galaxies evolve in terms of their morphologies and star formation histories, since the majority of the known galaxies in the nearby Universe are found to exist in groups. Compact groups of galaxies are of particular interest as they contain a small number of galaxies in dense configurations and host repeated interactions between them, enabling us to capture signatures of these interactions (e.g., tidal tails, shocks) for probing the underlying physics driving their evolution. While interactions themselves trigger intense star formation through gas inflows, compressive tides and turbulence, repeated interactions can spare no sufficient time for the galaxies to resume their normal star formation mode after their initial starburst and before the subsequent interactions. Such situations can dramatically affect the star formation regime of galaxies and give rise to three possible scenarios for subsequent interactions: a saturation effect in the star formation as the galaxies achieved high star formation rates already; a quenching effect where the initial interaction has stripped off the gas making it unavailable for forming further stars; a boost in starburst where the subsequent interactions are stronger than initial ones stimulating the burst itself. The aim of this project is to study the effect of repeated interactions on star formation in a compact galaxy group and Stephan's Quintet being one of the widely studied specimens in this context because of the remarkable tidal, hydrodynamic features (such as shockwaves resulting from galaxy collisions with the intragroup debris) and starburst episodes that it exhibits. However, reproducing all these features with a single hypothesized idea is challenging and the complexity in Quintet modeling necessitated modeling a simpler compact group of 3 galaxy members as the main focus is to understand the physics of star formation in repeated galaxy encounters. Stephan's Quintet and the general compact group are simulated using an adaptive mesh refinement hydrodynamic code RAMSES, the initial conditions for which are obtained using the MAGI code. To reproduce the features of the Quintet before exploring its physics, the model is simulated at a low resolution of about 1 kpc. Through the exploration of orbital parameter space, the proposed model resulted in some of the tidal features and the spatial locations of the galaxies to reasonably agree with observations, while the gas features such as the HI distribution outside the galaxies, separated stellar and gaseous tidal tails and the shock wave, could not be reproduced yet. Pertaining to the general group of 3 members, the simulations are performed at a resolution of about 12 pc with star formation and stellar feedback. The model considers an interaction of the main spiral galaxy with another spiral, shortly followed by another interaction of the main galaxy with an elliptical. A boost in starburst is observed by about 80-120 fold increase with respect to the star formation rate (SFR) prior to the interaction, in the central regions driven by gas inflows. Furthermore, the effect of interaction with the elliptical galaxy is not only causing an early onset of the starburst but also an enhancement in the SFR. Different orbital configurations that are less extreme than the initial are also considered. However, they do not yield quenching or saturation in the SFR either, but exhibit trends in the physics of star formation similar to that of the initial configuration. Furthermore, it is noticed that these starburst galaxies remain in an excited state (characterized by short depletion times) despite the SFR resuming pre-interaction values. I find that high velocity dispersion due to gas inflows and stellar feedback is the likely cause for this long-lasting excitation. In a general setting, the models discussed in this document are imperfect imitations of real galaxies in the sense that they do not incorporate all the physical phenomena on multi-scales, for example, Active Galactic Nuclei (AGN), an important feedback form in massive galaxies is not included. Therefore, high resolution models complemented with multi-wavelength and deep optical surveys revealing the signatures of repeated interactions in compact galaxy groups are needed to better constrain their interaction histories and thereby understand the physical processes governing their evolutions.

Contents

List of Figures

Chapter 1

INTRODUCTION

1.1 Galaxy evolution

Galaxies are observed to exhibit a wide range of morphological types and ever since Hubble proposed the tuning fork classification of galaxy types into ellipticals and spirals based on their shapes, a myriad of important questions about galaxies revolved around understanding the processes driving their evolutions into the configurations that we observe today. With the majority of the known galaxies residing in groups, interactions between them are crucial in shaping up their evolutions. Star formation, in particular, is important in this context as it determines major galactic properties like the colour, luminosity, chemical composition etc and interactions are known to trigger intense episodes of star formation in galaxies through mechanisms like gas inflows, compressive tides and enhanced turbulence. This project, therefore, aims at investigating the physics of star formation in repeated interactions specifically, where the galaxies would not have enough time to resume their quiescent SFRs in between the interactions by considering different compact galaxy group configurations.

1.1.1 Interactions

Environment in which galaxies reside is one of the significant factors impacting their evolution (Dressler, 1980). As majority of the nearby known galaxies exist in groups (Tully, 1987), interactions between them provide constructive insights into the galaxy evolution when compared to meagre galaxies in isolation. Such dynamical interactions between the members in spatially compact configurations are found to be powerful mechanisms in not just driving the morphological evolution (Moore et al., 1996) but also in triggering intense episodes of star formation (Larson and Tinsley, 1978). Cores of galaxy clusters and compact galaxy groups constitute such compact organizations, however, with a fewer number of galaxies per group (yet comparable number densities as that of cluster cores) and lower velocity dispersions of the members (as compared to clusters), compact galaxy groups enable easier and detailed analysis of the features resulting from interactions (e.g., diffuse optical features) and subsequently the analysis of underlying physics governing the group's evolution. Therefore, of all the other galactic organizations (like clusters and fields), compact galaxy groups that are dense configurations of small galaxy systems constitute ideal locations to investigate the physics of galaxy evolution. The first observational catalogs of compact galaxy groups (Rose, 1977 ; Hickson, 1982) and the subsequent surveys (Karachentseva and Karachentsev, 2000 ; Focardi and Kelm, 2002; Iovino et al., 2003) disclose a wide range of evolutionary stages spanned by compact galaxy groups from early interaction to advanced stages through observational evidence such as tails, shocks, HI maps etc (Fig 1.1). Such interactions between the galaxies can either lead to mergers or fly-bys depending on which of the two: dynamical friction or the velocity (relative) of interaction dominates the other. Accordingly, the interactions can result either in a massive giant elliptical embedded in hot gaseous halo called the fossil group (Ponman et al., 1994) or the galaxies separate from each other after flyby interactions, with tidal

Group	Credits
1. M81-M82-NGC3077	HI: VLA ; optical:DSS
2. NGC2992-93	HI: VLA ; optical:CTIO/SSRO
3. Stephan's Quintet	HI: VLA ; optical: HST (NASA)
4. The Mice	HI: VLA ; optical: HST (NASA)
5. The Guitar	HI: VLA ; optical: CFHT
6. The Antennae	HI: VLA ; optical: NOAO/AURA/NSF
7. The Atom for Peace	HI: VLA ; optical: ESO/WFC
8. NGC2623	HI: VLA ; optical: HST/NASA/ESA
9. NGC4694	HI: VLA ; optical: ESO/NTT

FIGURE 1.1: Optical images with overlapped HI maps (blue) of colliding galaxies at different stages of interactions (1 - initial stage to 9 - advanced) (Duc and Renaud, 2013)

dwarf galaxies likely to spawn in the tidal tails as a result of these interactions (Barnes and Hernquist, 1992 ; Duc and Mirabel, 1994). Since galaxies in compact galaxy groups have low velocity dispersions, dynamical friction typically would dominate and the groups are likely to merge into a fossil group ultimately.

1.1.2 Tides

An elementary step in understanding galaxy evolution in extreme environments is to unravel the individual interactions through observational evidence. Tidal tails constitute one of the obvious and striking features that persist for several hundred million years after the encounters and hold notable information about the nature of interactions. For instance, they point out their possible progenitors and their thickness could suggest an approximate time of occurrence of the corresponding interaction. While sharp features signify a recent encounter, diffuse and low surface brightness features tend to be results of older interactions since they would have had ample time to get diffused. Furthermore, tidal tails also provide clues to the galaxy types with tidal tails

noticeable only in spirals and not in ellipticals. Spiral galaxies have matter moving in an organized fashion where tidal perturbations on them translate into ordered features like tails. On the other hand, stars and gas in ellipticals move randomly and therefore the tidal perturbations on them are erratic resulting in diffuse structures instead (Duc and Renaud, 2013). Tidal tails, however, are not just signatures of dynamical interactions, but can also be important sites to probe the physics of star formation (Delgado-Donate et al., 2003) . Ever since the early observations by Zwicky (1956), the origin of these features has been highly debated for a long time. Tidal tails initially thought to be extraneous to tidal forces (Vorontsov-Velyaminov, 1962) are attributed to supernovae ejecta (Zwicky, 1962) and magnetic lines (Burbidge et al., 1963). However, subsequent numerical experiments revealed them to be purely gravitational phenomena caused due to differential gravitational forces acting on a galaxy due to another (Toomre and Toomre, 1972 (TT) ; Lauberts, 1974). Since the idea from these rudimentary numerical simulations, better models were made by considering dynamical friction (Gerhard, 1981 , but not included in TT), incorporating gaseous components (Noguchi and Ishibashi, 1986 ; Mihos et al., 1991) and taking a step further to investigate star formation related physics. Therefore, tidal tails essentially are the loosely bound matter (gas and stars) confined to the galaxy by a certain gravitational potential that gets modified during a close encounter with the perturbing galaxy resulting in its stripping from the host galaxy. While such disruptive tidal tails result from the early stages of interactions, tides are also found to be compressive at the peak interaction phase where these locations trigger the formation and prevent the dissolution of star clusters (Renaud et al., 2008).

The extent of stripping of the loosely bound matter, i.e the length and thickness of the tidal tails are dictated by several parameters such as mass ratio, proximity and duration of the interaction, relative velocities of the involved galaxies. One particular parameter associated with the duration of interaction is if the orbits are prograde or retrograde. In a prograde encounter, where the sense of a galaxy's rotation matches the direction of its orbital motion, gas and stars experience a prolonged perturbation from the perturbing galaxy, while in a retrograde encounter, the direction of galaxy's spin is opposite to its orbital motion and the perturbation experienced is for a shorter duration. Hence, prograde encounters are effective tidal tail builders while retrograde encounters do not result in prominent tails. Fig 1.2 shows one of my initial simulations of exploring the orbital parameter space in case of equal mass galaxies. The corresponding prograde and retrograde encounters exhibit the presence and absence of the tidal features respectively.

1.2 Star formation in the context of galaxy evolution

Star formation plays a crucial role in driving galaxy formation and evolution with its physics spanning a wide range of scales: from molecular clouds to galactic level. Although observations reveal intense star formation in interacting galaxies (e.g., The Antennae, Whitmore et al. 1999), the interplay between different processes contributing to this enhanced star formation is still poorly understood. Therefore, to precisely analyze star formation in the context of galaxy evolution, it is essential to capture mechanisms contributing to star formation on multiple scales (from sub-pc to kpc) with the aid of high resolution numerical tools.

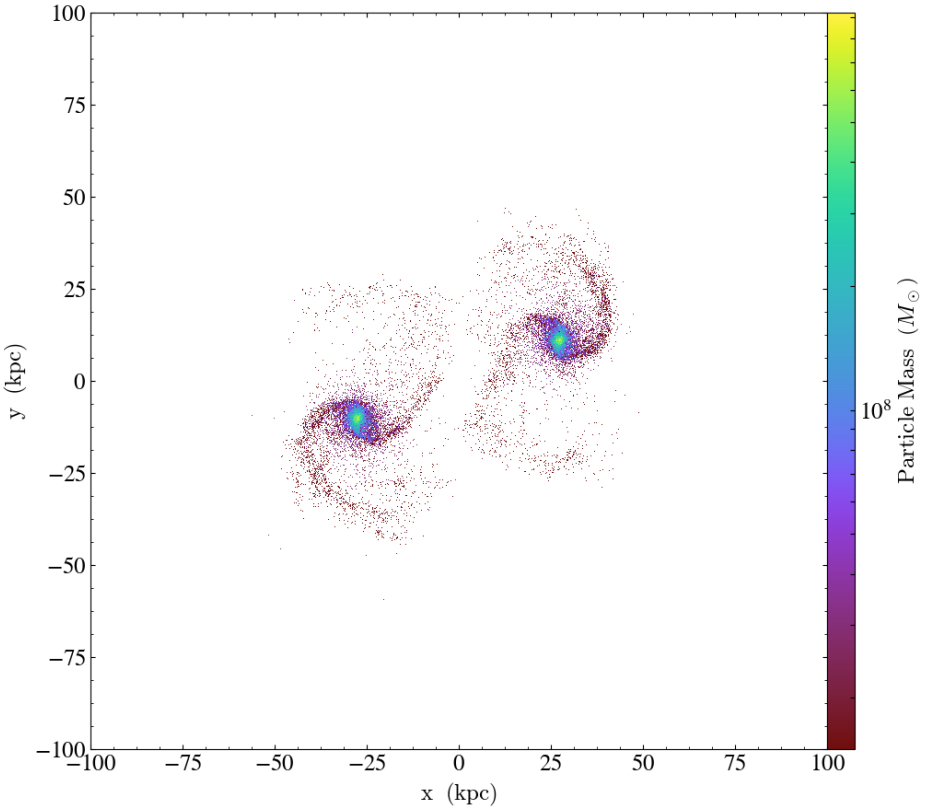

(A) Prograde encounter with noticeable tidal tails and bridges.

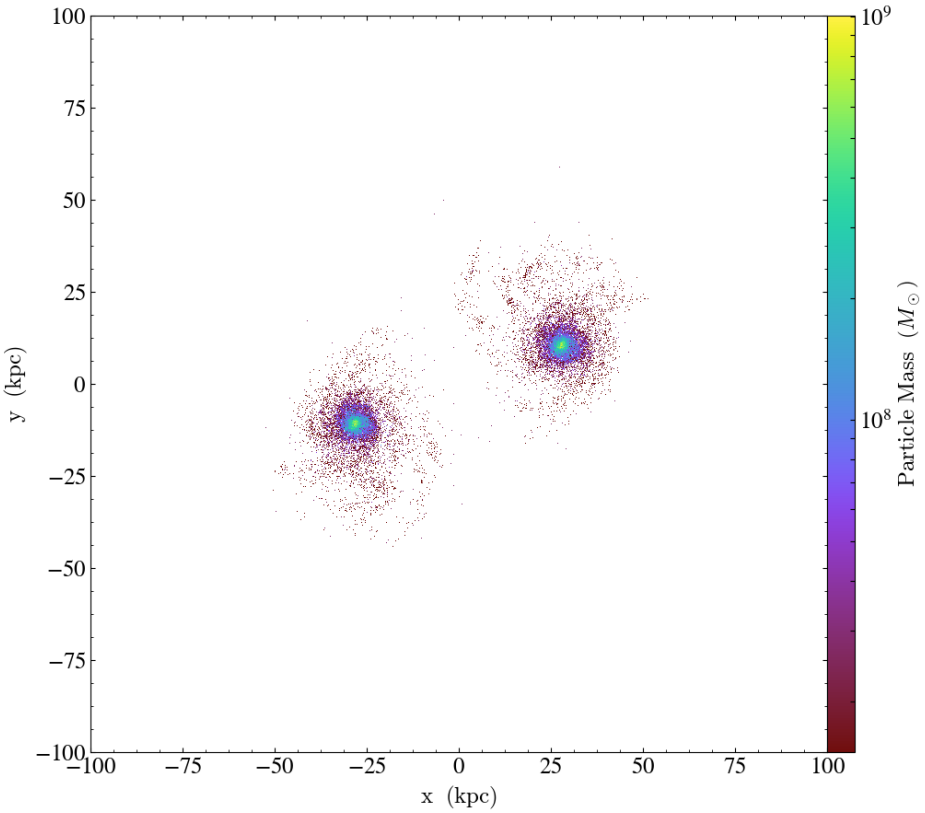

(B) Retrograde encounter where tidal tails and bridges are absent

FIGURE 1.2: Tidal tail formation in prograde and retrograde encounters from simulation of two equal mass galaxies (simulation method is described in Chapter 2). The plots are face-on matching with the plane of discs and orbital plane. The colorbar shows the projected stellar mass.

1.2.1 Kennicutt-Schmidt (KS) law and depletion time

On the galactic scale, an empirical relation between the surface density of star formation rate ($\dot{\Sigma_*}$) and surface density of the gas (Σ_{gas}) following a power law called Kennicutt-Schmidt relation (Fig 1.3) is widely adopted (Schmidt, 1959)

$$\dot{\Sigma_*} = A\Sigma_{gas}^{N} \tag{1.1}$$

Kennicutt (1998a) deduced the value of N to be $\sim$ 1.4 through HI and CO observations of $\sim$100 nearby galaxies. If a constant scale height is assumed, a theoretical explanation in support of this observational result is self-gravity, which expresses star formation rate density as the gas mass (exceeding Jeans mass) collapsing on a free fall time (τ_{ff}) that is proportional to $\rho_{gas}^{-0.5}$ (Elmegreen, 1994).

$$\dot{\rho_*} = \epsilon_* \frac{\rho_{gas}}{\tau_{ff}} \quad \propto \quad \rho_{gas}^{1.5} \tag{1.2}$$

where ϵ_* is local star formation efficiency (definition in section 2.2). However, a range of N (1-2) has been proposed in different literatures from the points of view of both observations (Sanduleak, 1969) and numerical simulations (Kravtsov, 2003), implying that measured SFR could be sensitive to the tracers considered (e.g., Hα, IR, UV) for its determination. Origin of such a scaling relation of star formation rate and gas density on a global scale is found to reflect the star formation behavior on small scales (Gnedin et al., 2014) and the correlation is found to be valid even down to the scale of giant molecular clouds (GMC) (Kennicutt et al., 2007 ; Bigiel et al., 2008). A consequence of star formation arising from this correlation is depletion time $\left(\tau_{dep} = \frac{M_{gas}}{SFR}\right)$: the time required for entire molecular gas to be consumed at its current SFR. For normal star forming galaxies, this spans a range of 2-10 Gyr, while τ_{dep} can dramatically drop in the cases of starbursts. This difference can be observed as two distinct regimes followed by normal disk galaxies and galaxies undergoing starburst in the Kennicutt-Schmidt plot (Fig 1.3). Although enhancement in star formation is widely observed and studied in interacting galaxies, the exact reason for such an enhancement is still obscure. Two evident possible reasons (from Kennicutt-Schmidt plot) are enhancement in availability of molecular gas and enhancement in the efficiency at which available gas is converted into stars, however, their individual contributions are still debated. While Pan et al. (2018) reports a lower enhancement in Star Formation Efficiency as compared to molecular H_2, Solomon and Sage (1988) & Sofue et al. (1993) notice that star formation is enhanced due to increase in Star Formation Efficiency, although molecular H_2 is not significantly increased. An increase in Star Formation Efficiency during interactions is also observed in Michiyama et al. (2016). Conversely, molecular gas content and not the efficiency is reported to be the dominant contributor to enhanced star formation by Combes et al. (1994) & Casasola et al. (2004).

1.2.2 Factors affecting star formation

Since star formation takes place on the scales of GMCs, understanding the processes favouring cloud formation and collapse will provide insights into understanding global star formation as well. Although, the basic effect involved is the collapse due to insufficient thermal and shear pressures to counteract gravity as the gas cloud exceeds a certain critical mass, several factors complexly affect star formation while their individual contributions still need to be probed thoroughly and this report attempts to understand how these factors shape the star formation in repeated galaxy interactions.

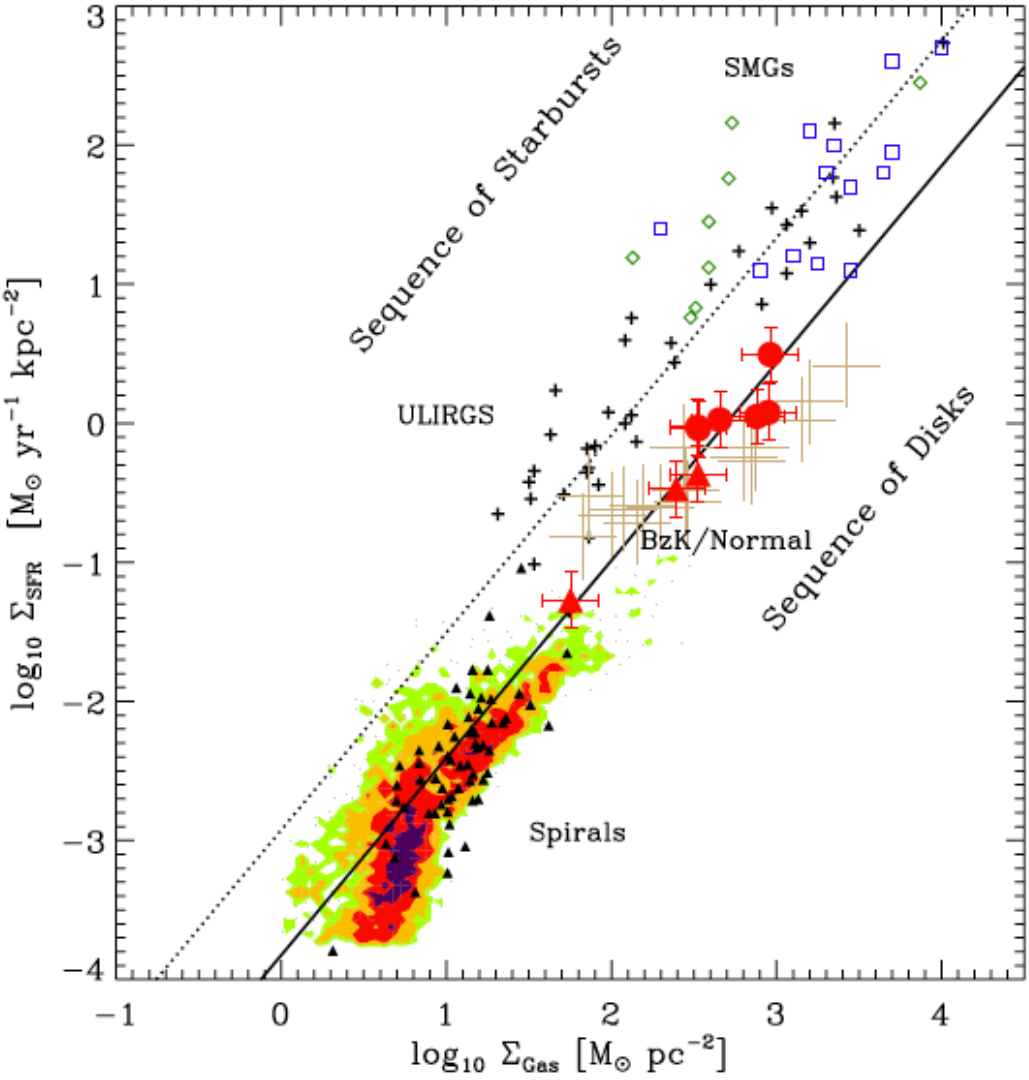

FIGURE 1.3: Kennicutt-Schmidt relation of surface density of star formation rate vs total gas surface density (atomic and molecular) in two distinct regimes: regular and starburst galaxies (ULIRG: Ultraluminous infrared galaxies and SMG: Submillimeter galaxies) from various observational surveys. The value of N, i.e the slope of the solid and dashed lines is 1.42 (Daddi et al., 2010a).

Gas response to external forces:
An obvious factor affecting star formation is the availability of dense molecular gas. Galaxy interactions favor star formation through shocks (Jog and Solomon, 1992), compressive tides (Renaud et al., 2014) and gas inflows towards the galactic nucleus (Bekki, 1995 ; Georgakakis et al., 2000). In a prograde encounter, gas inside the co-rotation radius of the host moves with angular velocity larger than the orbital angular velocity of the perturber and hence experiences a negative torque thereby losing angular momentum and spiraling in towards the center (Fig 1.4). Such kind of inflows also occur when the disc symmetry is disrupted due to formation of bars and spiral arms (Mihos and Hernquist, 1996). On the other hand, interactions in clusters and groups can lead to low HI content of the group due to ram pressure stripping (Gunn and Gott, 1972 ; Rasmussen et al., 2008) and strangulation effects (Kawata and Mulchaey, 2008) and tidal stripping of the gas, thereby quenching star formation.

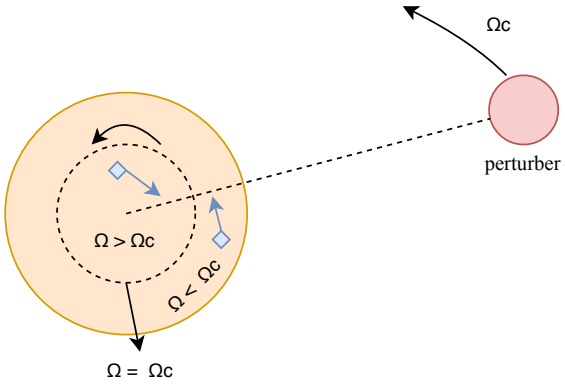

FIGURE 1.4: Gas inflows during galaxy interactions. Dashed circle represents co-rotation radius and the blue arrows inside and outside the co-rotation radius represent negative and positive gravity torques respectively.

Turbulence:
A fundamental problem observed with respect to star formation is that gas depletion time is much longer than the cloud collapse time (free-fall) (e.g.: Evans et al. 2009). So, some mechanism is responsible for the prevention of gas depletion and this was initially ascribed to strong magnetic fields (Shu et al., 1987). However, even more than magnetic fields, turbulence is found to influence star formation activity more effectively (Mac Low and Klessen, 2004). In a self-gravitating medium, turbulence can decelerate cloud collapse through increasing kinetic energy and at the same time is also capable of compressing the gas during shocks. While stellar sources contributing to turbulence include supernovae (SNe) and winds, numerical simulations (Agertz et al., 2009) point the main driving mechanisms of large scale turbulence to gravitational instabilities coupled with shear flows and tidal interactions (Kennicutt, 1998b) that cascade down to smaller scales. In Renaud et al. (2014), the turbulence is decomposed into compressive (curl-free) and solenoidal (divergence-free) components, where the compressive component, as the name implies, drives compression of the gas while solenoidal component is responsible for mixing of the gas through rotational effect. Their work finds an enhancement in the compressive component reflected as increased fraction of gas mass in higher densities corresponding to increased star formation during the galaxy interactions and this effect of compressive turbulence is . For isothermal and supersonic turbulent gas, the density probability distribution function (PDF) is known to follow a log-normal curve (Vazquez-Semadeni, 1994) whose width is found to primarily depend on the Mach number of the turbulence, M, (Krumholz and Thompson, 2007) as:

$$\sigma^2 \approx \ln\left(1 + \frac{3M^2}{4}\right) \tag{1.3}$$

With stronger turbulence (higher Mach number), width of this PDF increases, pushing significant gas fraction towards higher densities thereby facilitating star formation. This approximation of log-normal PDF of density is found to work well in both simulations (Bournaud et al., 2010) and the real systems (Berkhuijsen and Fletcher, 2008).

Feedback:
One of the crucial questions in understanding galaxy evolution involves our lack of comprehension of why galaxies are extremely inefficient at converting their gaseous mass into stars. While cooling promotes condensation of gas to form stars, it was found that the rate at which this happens in massive halos should produce more massive galaxies than we observe today (White and Rees, 1978). This means mechanisms to regulate the condensation come into play in the form of

feedback. While, SNe feedback and stellar winds are found to drive large fractions of gas as outflows to regulate star formation in dwarf galaxies (Efstathiou, 2000), massive ones require stronger feedback such as AGN jets and winds (Silk and Rees, 1998).

1.3 Starbursts in interacting galaxies

For a given stellar mass, certain galaxies are found to exhibit SFRs well above the main sequence galaxies (Fig 1.3). Such an enhanced star formation is attributed to physical processes usually occurring in dynamical interactions, where conversion of gas to stars is highly efficient (characterized by short τ_{dep}). Compact galaxy groups hosting repeated interactions between its members are ideal locations to witness such starbursts. However, how these bursts in star formation are affected during the subsequent interactions in repeated encounters depend on the properties of the interaction and the gas response, giving rise to three possible conditions as discussed below.

Boost in starburst:
In a repeated galaxy interaction scenario, where the galaxies experience encounters so frequently that they do not have enough time to resume their normal star formation mode before subsequent interactions, a burst in starburst itself can occur if the subsequent interactions can drive the already excited galaxy to form stars at even higher rates. This efficient star formation could be due to stronger compressive tides, gas inflows, gravitational instabilities arising from formation of stellar bars and spiral arms. For example, Teyssier et al. (2010) reports a boost of SFR enhancement in simulations of Antennae-like galaxy mergers (Fig 1.5) and attributes the central concentration of starburst to gas inflows. However, the induced starburst during interactions is not restricted to central regions, but extended star formation is also observed that is inexplicable through just gaseous inflows. Moreover, Wang et al. (2004) finds that presence of abundant molecular gas at the centers is necessary but not sufficient for star formation, as The Antennae exhibit lower central star formation as compared to off-center regions. This implies a possible requirement of additional triggers such as shocks, compressive tides and compressive turbulence to be invoked in order to explain extended star formation.

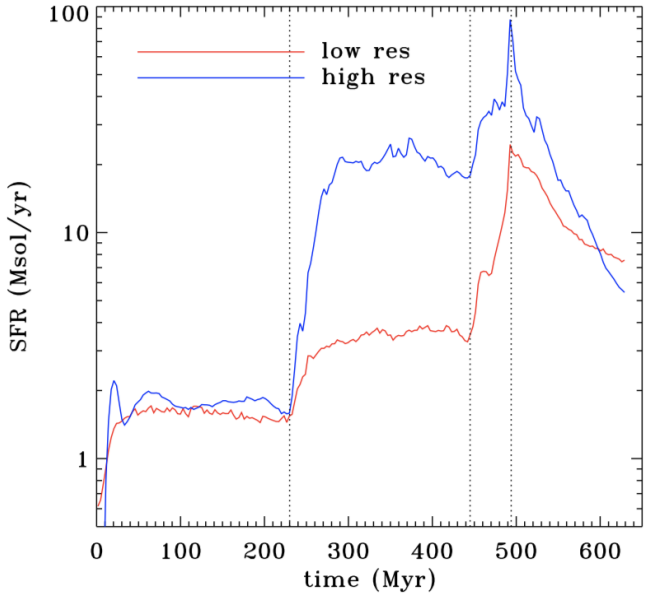

FIGURE 1.5: Galaxy pair merger simulated at low (96 pc) and high resolutions (12 pc) from Teyssier et al. (2010) exhibiting enhancement in star formation after the second pericenter passage (vertical lines).

Saturation:
On the contrary, some of the simulations have reported the majority of interactions resulting in a weak enhancement in the star formation (Di Matteo et al., 2008) that is consistent with observations (Bergvall et al., 2003 ; Jogee et al., 2008). For example, Di Matteo et al. (2007) presents more than 200 simulations of interacting galaxies and mergers only to find about 17% of them exhibiting strong starbursts. They conclude that for gas-rich galaxy interactions, inflows are inefficient contributors to starbursts in contrast to the disc fragmentation arising due to instabilities. However, the latter activity not necessarily triggered by interactions. Perret et al. (2014) simulates gas rich galaxy interactions at the epoch of peak in star formation (1<z<2) and surprisingly finds no starburst in both major and minor merger events possibly due to their implementation of cooling mechanism. A more recent work, Fensch et al. (2017), arrives at a similar conclusion through comparison of the galaxy interactions in case of low gas fraction and high gas fraction and finds that the factors effective in driving starbursts in low gas fraction case (turbulence, compressive tides and gas inflows) only mildly enhance SFR (Fig 1.6) in high gas fraction which is already high in the pre-interaction stage itself ($\sim$ 60 times pre-interaction SFR in low gas fraction). While galaxies with high gas fraction are "excited" (i.e exhibit high SFRs, as opposed to low gas fraction galaxies) even prior to the interactions, another way to achieve such excitation particularly in low redshift galaxies is through repeated galaxy encounters.

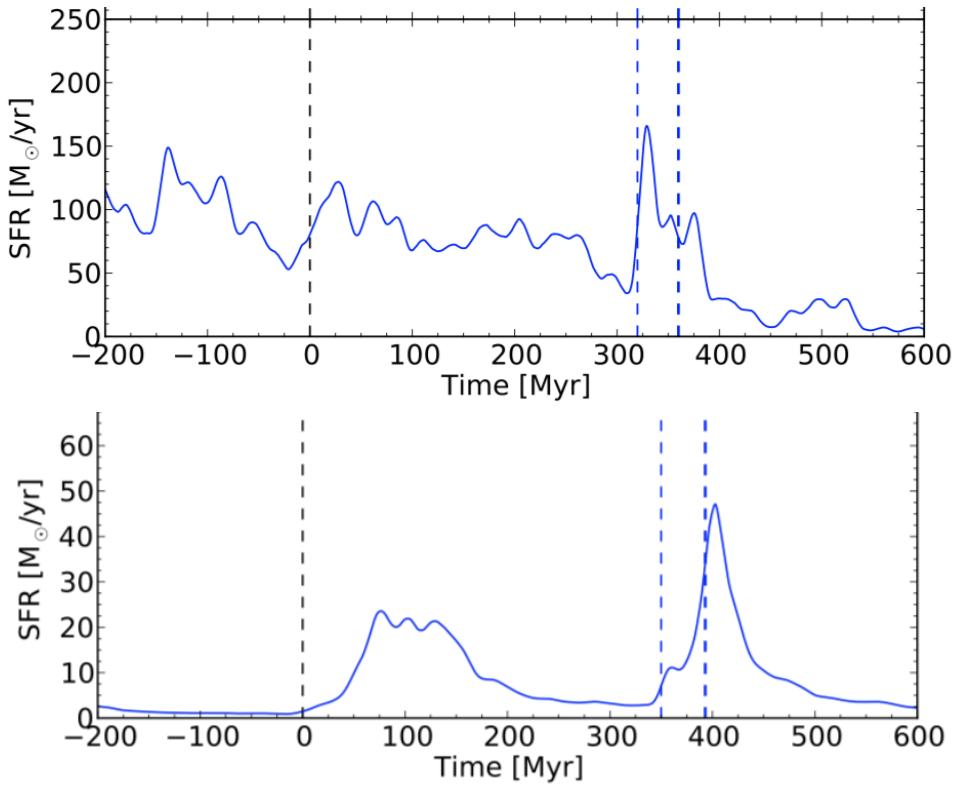

FIGURE 1.6: Top panel: Saturation effect in SFR for galaxy interaction of high redshift galaxies ($f_{gas} \approx 60\%$) ; Bottom panel: Significant boost in SFR from the pre-interaction stage in low redshift galaxies ($f_{gas} \approx 10\%$), both from Fensch et al. (2017). The dashed lines correspond to first, second pericenter passages and final coalescence.

Quenching:
An extreme effect of interactions in compact galaxy groups could be quenching of star formation (e.g. Fig 1.7) right after the first pericenter passage when no more gas is available for further star

formation and hence star formation ceases abruptly. The standard quenching scenario in dense environments involves tidal stripping of cold gas during interactions, however, stripping of gas is not necessarily the only way to quench star formation in interactions. One such quenching mechanism that doesn't involve the removal of gas, called morphological quenching, is discussed in Martig et al. (2009). During interactions, the disc of a star forming galaxy can be disrupted into forming a diffused blob of gas. Due to lack of dense gas, the star formation in the galaxy is ceased until the diffused structure settles down into a disc again. It is also possible that shocks during interactions can drive disruptive turbulence that can lead to quenching as they prevent the molecular gas from getting dense enough to form stars (Alatalo et al., 2015).

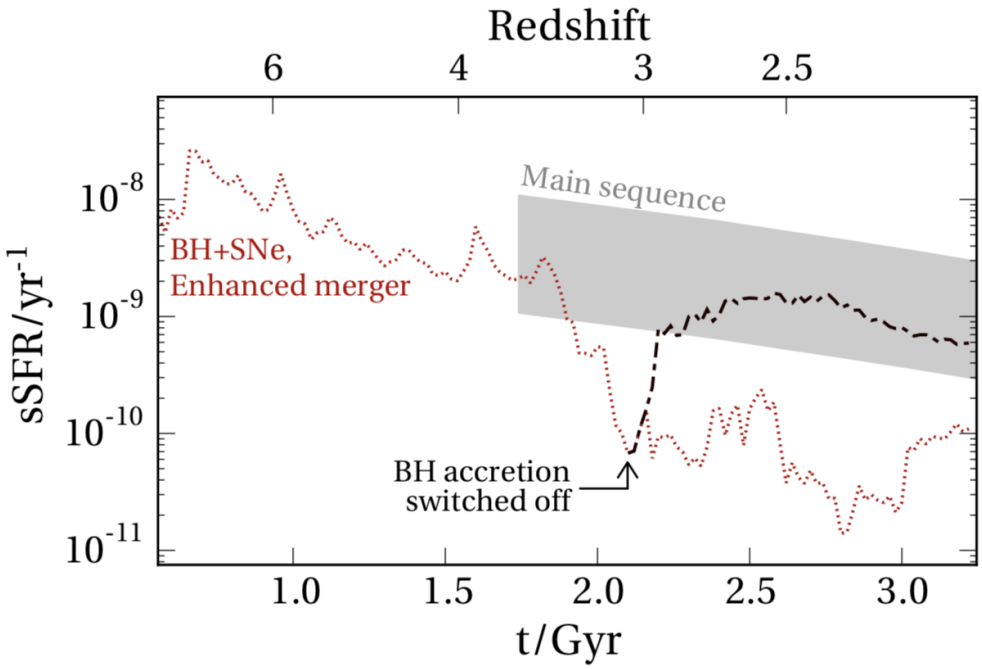

FIGURE 1.7: An example of Quenching in mergers from Pontzen et al. (2017). The plot shows the effect of a black hole in maintaining the quenched state of the merger while turning it off drives the merged galaxy into normal star forming regime (black dashed line).

The examples of above described scenarios correspond to the simplest interactions between galaxy pairs. Pairs are insufficient to mimic extreme conditions which requires the duration between interactions to be much smaller than the starburst duration. On the other hand, extreme conditions are frequent in compact galaxy groups due to their compact spatial configurations resulting in repeated violent interactions. Resorting to such dense environments and elevating the galaxies to excited states through interactions (i.e, high SFRs: comparable to the initial conditions as that of galaxies with high gas fraction), would the subsequent interactions give rise to a similar saturation effect as noticed in Fensch et al. (2017) due to unavailing effect of the interactions on galaxies' already excited states, or do we expect the other two situations (Quenching and Boost of starburst)?

The objective of this project, therefore, is to understand the physics of star formation in the context of galaxy evolution through repeated interactions where the galaxies still remain in the excited state right before the subsequent encounters.

Chapter 2

METHOD

While observations of galaxy systems provide limited information, such as the morphology and features resulting from the past and on-going interactions, numerical simulations are the most useful tools to test our hypotheses of possible formation scenarios and to understand the underlying physics leading to the current configurations. The compact galaxy groups simulated in this report are considered to be at low redshifts with compact spatial volume (max $\sim$ 2 MPc^3) and short interaction timescales (max $\sim$ 1 Gyr). Hence, the Hubble expansion can be neglected and the simulations are run in a non-cosmological context without any gas accretion.

2.1 MAGI

MAny component Galaxy Initializer (MAGI) (Miki and Umemura, 2017) is an initial condition generator used to generate galaxy models through user specified profiles, masses and scale lengths of the individual components. MAGI not only creates dynamically stable particle systems, but also allows the creation of multiple components in galaxies (bulge, gas & stellar discs, dark matter halo). All these components of galaxies comprising of stars, dark matter and gas are generated as ensembles of particles in MAGI, however, when passed to RAMSES, gas particles get replaced and are deposited onto the computational grid, while the stars and dark matter remain as particles. MAGI employs distribution function based approach to compute the initial conditions of the particles. It calculates the Eddington's distribution function (Eddington, 1916), a function of energy, from which particle velocities are obtained by rejection sampling and the positions from the potential through inverse-function sampling. In this work, all the spirals galaxies are modeled with a Hernquist bulge (Hernquist, 1990), Exponential stellar and gas discs and an NFW profile for halo (Navarro et al., 1996), while the ellipticals are devoid of the stellar disc and the profiles remain the same for the other components. While NFW profile is a standard choice for dark matter halos, in addition, it also prevents the development of non-axisymmetric structures and the subsequent central gas flows in the disc galaxies which makes it convenient to analyze central gas flows caused due to interactions. Masses of the individual components for each galaxy are obtained from the following constraints:

$$\begin{aligned} &\text{cosmological baryon fraction} , \ \frac{M_{baryon}}{M_{baryon} + M_{dm}} \sim 0.17 \ [1] \\ &\text{gas fraction} , \ \frac{M_{gas}}{M_{baryon}} \sim 0.1 \\ &M_{disc} \ \alpha \ r^2_{scale,disc} \end{aligned} \tag{2.1}$$

However, the above mentioned gas fraction is valid only for the spirals, while the gas-poor ellipticals are considered to have a negligible gaseous component.

[1] Bennett et al. (2013)

2.2 RAMSES

RAMSES (Teyssier, 2002) is an Adapative Mesh Refinement hydrodynamical code enabling us to execute simulations at spatial resolutions high enough to capture complex physics occurring on different scales. However, resolving the entire computational domain at the maximum resolution is computationally expensive as well as unnecessary. The technique of Adaptive Mesh Refinement (Berger and Colella, 1989), where the grid is adaptively refined (de-refined) to higher (lower) resolutions only in locations where there is higher (lower) mass density is therefore optimal due to utilization of both memory and the computational time as required. The time step in the simulations is also adaptive and is determined through Courant-Friedrichs-Lewy condition. This condition imposes a constraint on the time step so that the information (e.g. a star or a dark matter particle) in a cell travels only to its immediate neighbour in the grid during this step.
The stars and dark matter in the simulations are treated as particles of different mass resolutions in a collisionless system and the corresponding gravitational equations are solved using a Poisson solver. On the other hand, the gas is described on the grid and the hydrodynamics is treated using Eulerian approach, where the fluid properties are analyzed at a given point in space as a function of time. The corresponding conserved equations of mass, energy and momentum are solved using a second-order Godunov method which uses Reimann solver to obtain fluxes across the grid cells. All the parameters necessary for the physics and initializing the simulation are supplied through a parameter file.

1. Mesh refinement parameters:
The box length (`boxlen`), coarse level (`levelmin`) and fine level (`levelmax`) determine the minimum $\left(\frac{\texttt{boxlen}}{2^{\texttt{levelmin}}}\right)$ and maximum $\left(\frac{\texttt{boxlen}}{2^{\texttt{levelmax}}}\right)$ resolutions, and these parameters stay unchanged throughout the simulation. However, to control the refinement levels attained during the simulation, two additional parameters are defined: `mass_sph` and `m_refine` such that refinement of the grid cell is done only when the baryonic mass in it exceeds `mass_sph` * `m_refine` or the number of particles in the cell exceed `m_refine`.

2. Cooling and Heating:
The thermodynamic model for heating and cooling of gas in this work are ascribed to the ultraviolet background from massive stars (Haardt and Madau, 1996) and atomic/molecular lines (Courty and Alimi, 2004) respectively. The cooling strongly depends on the metallicity of the gas. Hence gas with a high metallicity is prone to cool efficiently since metals are easily excited/de-excited due to their compact energy levels. The initial metallicity considered throughout this entire work is solar and the ISM is enriched with metals eventually through metal deposition during feedback.

3. Star formation:
In the simulation, two parameters essentially allow us to control the star formation. A density threshold to set how dense the gas in the cells should get in order to collapse to form stars and the efficiency with which this gas is converted into stars. The density probability distribution function of gas that describes the distribution of galactic gas in various densities (ranging from diffused halo to dense star forming gas) can be used to determine the density threshold. Star formation efficiency (different from the global efficiency discussed in the introduction section corresponding to Kennicutt-Schmidt plot) in each cell is defined as the fraction of gas mass converted to stars $\left(\epsilon = \frac{M_*}{M_{gas}+M_*}\right)$, M_* here being the mass of newly formed stars. Typical values of star formation efficiency for sample Giant Molecular Clouds in the Milky Way are noted to be about 1% - 10% (Murray, 2011 ; Evans et al., 2014). The density threshold and efficiency are scale dependent, with the density threshold being higher for simulations with higher resolutions. Both these parameters

are to be adjusted to get a reasonable SFR and locations of star formation. For instance, a combination of high threshold-high efficiency and a low threshold-low efficiency can result in the same SFR, however, the former can lead to concentrated star formation due to stars spawning only in regions of high densities while the latter would form stars in extended regions of low densities as well.

The model for star formation is adopted from KMT09 (Krumholz et al., 2009a ; Krumholz et al., 2009b). To compute the fraction of molecular hydrogen (f_{H_2}), this model considers a balance between the formation of H_2 molecules on the dust grains in atomic-molecular gas complexes and the molecules' photo-ionization due to UV radiation.

$$f_{H_2} = 1 - \frac{3}{4}\frac{s}{(1 + 0.25s)} \tag{2.2}$$

where s encompasses the intensity of dissociating radiation and number density of the gas which in turn depends only on the gas metallicity (the solar metallicity, $Z_\odot$ in our case which represents low redshift galaxies of the considered masses). The volume density star formation rate per cell is then given by:

$$\dot{\rho_*} = f_{H_2}\frac{\rho_{gas}\,\epsilon}{t_{ff}}; \quad \rho_{gas} > \rho_{threshold} \tag{2.3}$$

where ρ_{gas} is the gas density in the cell, ϵ is the star formation efficiency in each grid cell (not to be confused with the global star formation efficiency in the context of Kennicutt-Schmidt law) and t_{ff} is the free fall time of collapsing gas cloud. With the density threshold criterion met, at every time step, the gas mass that is converted to stars is then calculated as a ooduct of number of star particles (n_*), a random number generated from a Poisson distribution and the constant mass of a star particle (M_*).

4. Feedback:
To regulate star formation, this work takes into account the types of stellar feedbacks described in Agertz et al. (2013): radiation pressure, stellar winds and supernovae in the forms of energy, momentum, mass and heavy metal injection onto the grid.

Radiation pressure: The feedback due to radiation pressure in the simulation is described through momentum injection resulting from direct absorption and scattering of the IR radiation (η_1) as well as momentum transfer by re-radiated photons (η_2).

$$\begin{aligned} \dot{p}_{rad} &= (\eta_1 + \eta_2\tau)\frac{L_*}{c} \\ p_{rad} &= \dot{p}_{rad}\Delta t \end{aligned} \tag{2.4}$$

where c is the speed of light, Δt is the simulation's fine time step, τ is the optical depth in IR and L_* is bolometric luminosity of a stellar population. This luminosity is the product of total mass of star particles in a cell younger than a particular age (6 Myr in this work) and the specific luminosity (Fig.1 in Agertz et al. 2013). An important point to note here is that since the individual stars are not resolved, a single stellar particle is assumed to be a collection of stars obeying a certain Initial Mass Function (Chabrier, 2003).

Stellar winds: Feedback contribution from stellar winds of young massive stars operates on the similar timescale of radiative pressure ($\sim$ 6.5 Myr) and is incorporated through energy (E_w), momentum (p_w), mass (m_w) and metal (m_{z_w}) injections. They are approximated as functions of metallicity (Z), age of stellar population (t_* in Myr) and birth mass of star particle (m_{*b} in $M_\odot$) in the following manner:

$$E_w = m_{*b} * (1.9 * 10^{48}) \left(\frac{Z}{0.01}\right)^{0.41} \frac{t_*}{6.5} \text{ erg} \tag{2.5}$$

$$p_w = m_{*b} * (1.8 * 10^{40}) \left(\frac{Z}{0.009}\right)^{0.36} \frac{t_*}{6.5} \text{ cm/s} \tag{2.6}$$

$$m_w = m_{*b} * (0.024) \ln\left(\frac{Z}{4.6 * 10^{-4}} + 1\right) \frac{t_*}{10} M_\odot \tag{2.7}$$

$$m_{z_w} = Z m_w M_\odot \tag{2.8}$$

Supernovae: Supernova feedback includes both type II and Ia injected in the form of energy, momentum, mass and metals. While the energy, ejected mass and metal mass are injected into 27 surrounding cells (including the cell of the stellar particle), momentum is either directly injected through velocity kicks into the neighboring cells (excluding the cell containing the stellar particle or by adding non-thermal pressure calculated from momentum flux across the cells to the thermal pressure. From the IMF and given age, the masses of stars leaving the main sequence are computed. The supernovae are considered type II if the mass range is > 8 $M_\odot$ and type Ia otherwise. The energy contribution from supernovae is then $E_{SN} = \#SN * 10^{51}(\text{ergs})$ assuming same energy (10^{51}) released in both the cases. The number of supernovae, #SN, occurring at time step Δt is obtained by integrating the IMF over the mass ranges that leave their main sequences at that time. The mass ejections in SNe are computed as follows (from Raiteri et al., 1996, except m_{ej}):

$$m_{ej} = 0.5 * M^{1.06} \tag{2.9}$$

$$m_{Fe} = 2.8 * 10^{-4} M^{1.864} \tag{2.10}$$

$$m_O = 4.58 * 10^{-4} M^{2.72} \tag{2.11}$$

In addition to the above mentioned momentum release in the initial stages of the supernovae, significant momentum is injected in the later stage (Sedov-Taylor phase, p_{ST}) due to adiabatic expansion of the shockwave (e.g., Ostriker and McKee, 1988).

$$p_{ST} = 3 * 10^5 \, E_{51}^{16/17} \, n_o^{-2/7} \tag{2.12}$$

where E_{51} is the thermal energy in units of SNe energy and n_o is ambient density. Pertaining to SNIa, the feedback is through energy and mass ejections in a similar way as for SNeII. Finally, a fraction of total feedback energy (50%) that can be perceived as contributions from magnetic fields and cosmic rays and is supplied as a separate variable (Jubelgas et al., 2008 ; Wang and Abel, 2009).

This report discusses two compact galaxy group models: Stephan's Quintet, a 5 membered group (more details provided later in the text as well as in the appendix), the simulation for which is performed isothermally at a resolution of $\sim$ 976pc (`boxlen`=2Mpc ; `levelmax`=11) with no star formation, feedback or cooling included, since the initial focus is to obtain approximate morphology of the quintet, before investigating the physics of the group. Due to the complexity of this task, we also look at the second model, a 3 membered general group (details tabulated in the appendix), for which the physics described above is investigated at a maximum resolution $\sim$12pc

(`boxlen`=0.4Mpc ; `levelmax`=15) to accurately resolve the physics even on small scales. The system is first allowed to evolve isothermally at 10^4K for $\sim$ 120 Myr at a lower resolution ($\sim$ 48pc), after which the cooling phase is commenced with increased resolution ($\sim$ 24pc), lasting for $\sim$ 20 Myr to ensure that changes in the dynamics are only due to the heating/cooling sources. The third stage is when the cooling is kept intact and the star formation and the feedback are triggered at the same time at the maximum attainable resolution. Star formation and feedback for this model are triggered when the density threshold 50 H/cc is reached and star formation efficiency of 5% is considered and this yields an initial SFR of $\sim 5 M_\odot$/yr for the entire system.

Chapter 3

RESULTS

In this section, I first present the results of modeling a specific compact group: Stephan's Quintet and discuss the hypotheses for its possible formation scenario using observational constraints and thereby the reproduced features. I then look at the need for modeling a more generic compact group and investigate the physical drivers and properties of the obtained starbursts.

3.1 Introduction to Stephan's Quintet

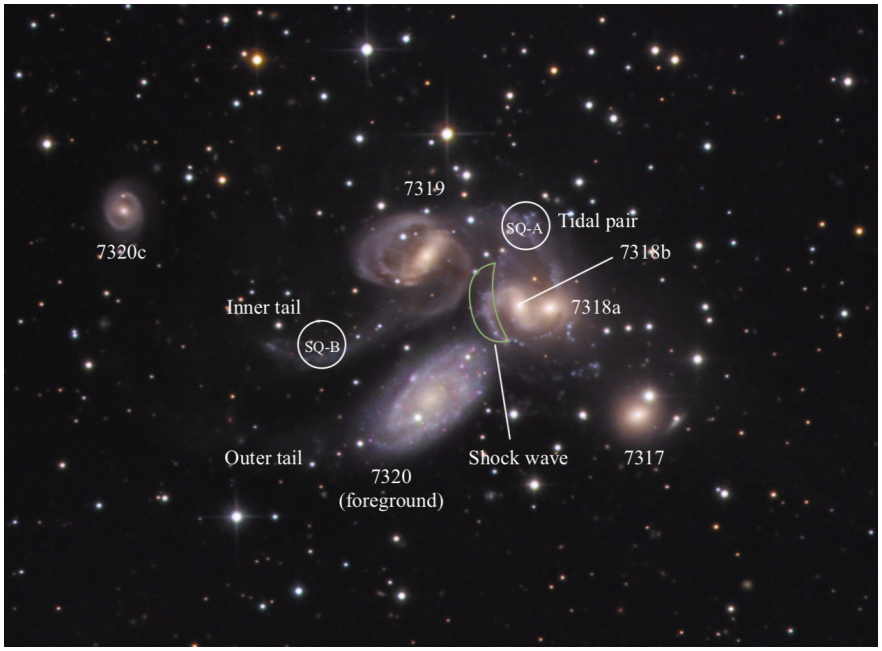

FIGURE 3.1: Optical features of Stephan's Quintet with starburst regions, SQ-A and SQ-B observed in UV and the shockwave being observed in X-ray marked. Left of the figure is East and Top is North. (Credits: Johannes Schedler, CCD-Guide)

Stephan's Quintet is an interesting example of a compact galaxy group to understand the physics involved in extreme environments as it is at an important stage of its dynamical evolution exhibiting striking features resulting from its past and current interactions. The system is the first discovered compact galaxy group consisting of 5 NGC members [2]: 7319 (main), 7317, 7320c, 7318a and 7318b at a distance of ∼94 Mpc (z∼0). However, the galaxy, 7320 in the quintet's optical images is in the foreground and doesn't belong to the group and this is known from 7320 having a lower radial velocity than the Quintet's members. The system is subjected to observations in a variety of wavelengths spanning from X-rays to radio, each revealing interesting features. While optical images exhibit tidal features such as tails extending from the main galaxy: One faint and diffuse while the other bright and narrow, and a crossed pair of tails emanating from 7318a and 7318b (see Fig 3.1), HI maps (Williams et al., 2002) have revealed the presence of most of the

[2]NGC is omitted in the subsequent parts of the report when referring to the members of the quintet.

group's neutral gas outside the galaxies. On the other hand, a shorter wavelength range observations of X-rays (O'Sullivan et al., 2009) revealed the energetic features in the group such as the shockwave resulting from the high speed ($\Delta v_r \sim 900$ km/s) intruder's (7318b) interaction with the inter-stellar medium and stellar debris and an AGN in the main galaxy's nucleus. Probing the system in UV has revealed locations of starbursts in the group as a result of the violent interactions between the members (Xu et al., 2005).

Based on the clues from the above observations and kinematics, attempts have been made to numerically model the quintet, reproducing the morphology and to understand the underlying physics. A gas free N-body simulation has been performed in Renaud et al. (2010) however, the model couldn't explain hydrodynamic related features such as the shock wave and HI profile, as it did not include gaseous components. An extension to the N-body model was a hydrodynamical model employing smooth particle hydrodynamics simulated in Hwang (2010). Although SPH modeling is simple due to its mesh-free formalism, this particle based approach has a poor ability to capture discontinuities without introducing an artificial parameter to account for the necessary energy dissipation. Such discontinuities are readily produced in the Eulerian approach and hence, the latter can be a promising method to accurately explain features like shock waves. Furthermore, recent deep optical images of the Quintet, acquired from the Canada-France-Hawaii-Telescope (CFHT), an instrument with high sensitivity and a wide field of view, have however revealed additional features that are of low surface brightness and haven't been detected in the observations before (Duc et al., 2018) (Fig 3.2). These features include:

- An off-centered diffused halo around 7317 implying a previous interaction between the galaxy and the group (labelled A in Fig 3.2).
- The outer tail visibly pointing towards the galaxy, 7320c (labelled B in Fig 3.2).
- Bifurcation of the inner tail (labelled C in Fig 3.2).

FIGURE 3.2: Deep optical image of the quintet revealing low surface brightness features taken from Duc et al. (2018)

3.2 Exploration of parameter space for Quintet formation:

Taking into account the newly unveiled features in addition to the already observed ones, I first propose a possible formation scenario of the system based on a timeline of the interaction events constrained by the surface brightness of the features and the ages of star clusters (Fedotov et al., 2011). Lowest surface brightness features would have formed earlier as they would have had enough time to diffuse and hence, the off centered halo and the faint branch of the inner tail would have formed first followed by the outer tail. However, unlike the other tidal features, there is no observational evidence to constrain the age of stars in the diffused halo yet, and since the older features are prone to fading and destruction through subsequent interactions, it is difficult to determine the exact time of the interaction. For such a situation, the final model of the group built from the other observational hints can help to backtrack the possible interaction time of such older structures. The deep optical observations clearly reveal the progenitors of these two interactions to be 7317 and 7320c respectively. The next interaction in the line is the one responsible for the inner tail formation. Unlike the former interactions, optical images do not reveal a clear progenitor. However, other numerical simulations, e.g., Renaud et al. (2010) have tried to associate the inner tail to a second encounter with 7320c, but couldn't reproduce the morphology because of too strong dynamical friction that would have resulted in a merger. Therefore, in this model, I consider a possibility for the formation of sharper branch of the inner tail to be the interaction of the main galaxy with 7318a instead. And finally, the crossed pair of tidal tails are the consequence of the interaction between 7318a and the high speed intruder 7318b moving towards us and currently thought to be plunging into the group with a velocity of ~ 900 km/s with respect to other members. The described model is illustrated in Fig 3.3 and assumes that no merging event has occurred yet. Another note is that, since reproducing the quintet morphology is focused at the features of the group on a broad scale, obtaining detailed inner structures of the individual galaxies (such as the central bars and orientation of the galaxies) remain out of scope of this work.

The types of the galaxy members are deduced from the optical images with the ones exhibiting tidal features regarded as spirals (see section 1.1.2). The main galaxy, 7319, is considered to be similar to Milky Way in terms of the scale radii of components and the other galaxies are scaled with respect to 7319 through visual inspection. The initial conditions and orbital parameters for the system are obtained through initial exploration of parameter space as discussed below and fine-tuning them further through trial & error and the final parameters are tabulated in the appendix (Table A.2). In this process of obtaining the Quintet's morphology, I found three parameters to be effective in shaping the formation scenario from the proposed model to the final stage of resembling the observations. These are: eccentricity of the orbits, directions of the spin and the pericenter passages.

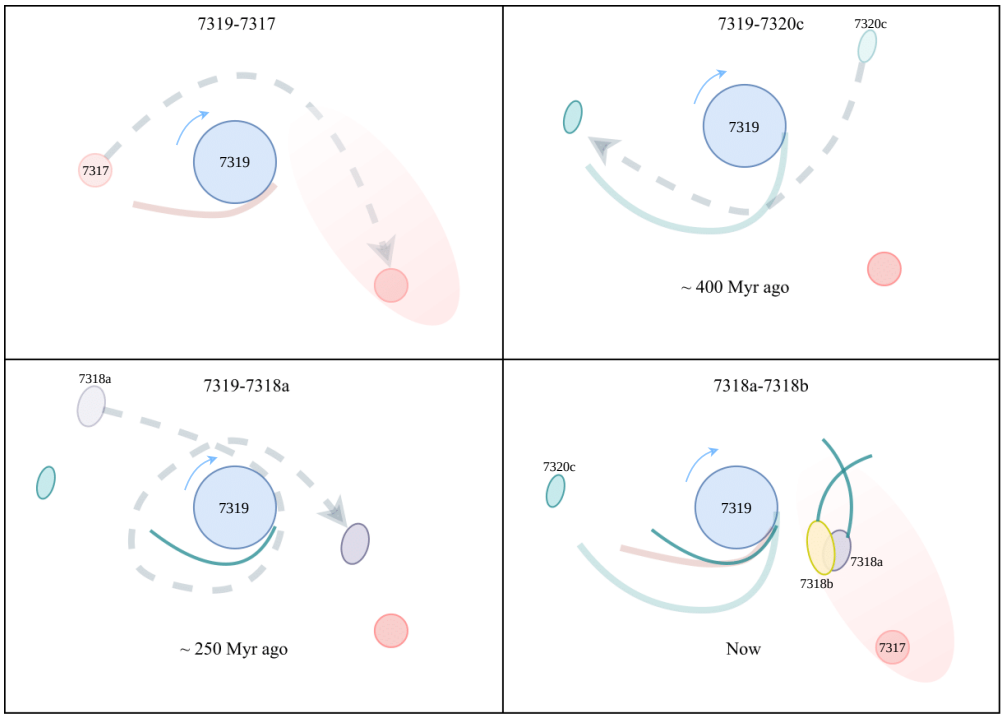

FIGURE 3.3: Model hypothesis for the Quintet's formation with 7319 considered to be the main galaxy. The extended diffuse structure in the first and final panels represent the off-centered diffuse halo and the timeline is proposed in accordance with the stellar cluster ages from Fedotov et al. (2011). The first interaction lacks the information of star cluster ages and hence its time of occurrence is unknown at the current stage, however, the final model could provide hints about this epoch. Galaxy sizes and distances not drawn to scale.

Eccentricity:
Orbital eccentricities of galaxies play an important role in steering the merging process during interactions. While orbits with low energy and low angular momentum (elliptical and certain parabolic, hyperbolic orbits) lead to mergers as tidal interactions transfer the orbital energy to internal energy, orbits with high enough angular momenta and eccentricities lead to fly-by interactions. This is the basis of first interaction step in the simulation where a parabolic orbit at a given pericenter appears to lead to a potential merger (Fig 3.4), while a hyperbolic orbit of eccentricity 3 yielded a wide separation and the required off-centered diffuse halo (Fig 3.5). However, the tidal tail corresponding to the bifurcated branch is reversed in its orientation (shown inside the ellipse of Fig. 3.5)

Spin:
The orientation can be fixed by flipping the spin of main galaxy, however, with the current orbit, reversing the spin will make the encounter retrograde. To be still able to form the tail, the orbit of 7317 should also be modified accordingly (a prograde encounter is required for the tail formation). However, doing so, produces the tail in the required orientation but a mismatch in the observed halo (Fig 3.6). The proposed model therefore poses a trade-off situation between the tail and the halo and it is chosen to retain halo and compromise on the bifurcation of inner tail that could be attributed to a different factor (e.g., one of the subsequent interactions). Now that the spin of the main galaxy has been changed, original orbit of 7320c will not result in a tail anymore unless the orbit is changed to prograde.

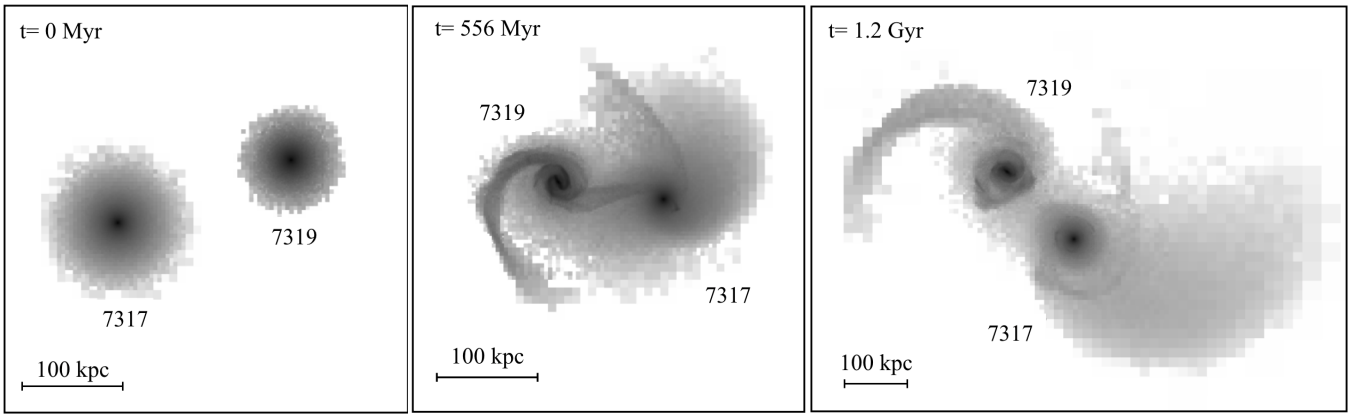

FIGURE 3.4: Parabolic encounter of 7319 with 7313 exhibiting a potential merging activity. The maps in grey from here on are projected stellar density in $M_{\odot}/kpc^2$ with the color range (10^{-3} [lightest], 10^{10} [darkest])

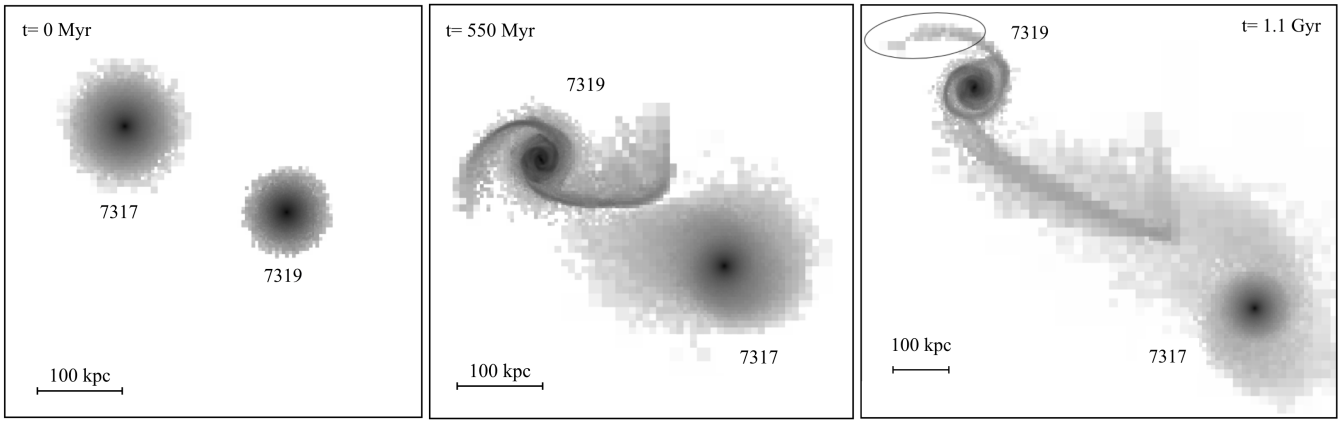

FIGURE 3.5: Hyperbolic encounter of 7319 with 7313 that produces an off centered diffused halo with no signs of imminent merging.

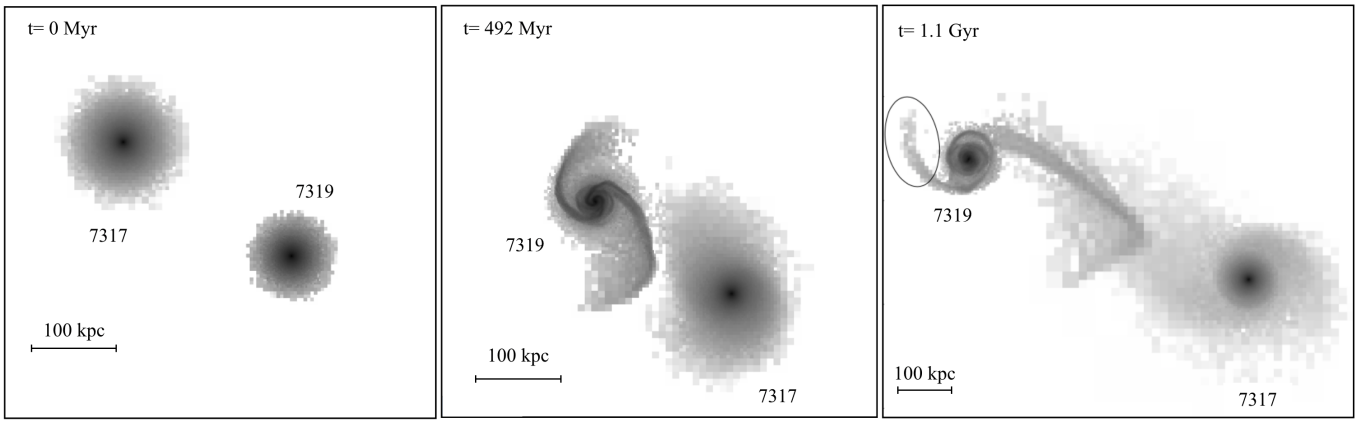

FIGURE 3.6: Modified hyperbolic encounter of 7319 with 7317 to produce the tail in the correct orientation.

Pericenter passage:
Distance of pericenter passage is a parameter observed to influence the length of the tidal tails . A shorter pericenter passage resulted in a shorter tail (Fig 3.7) due to a transient interaction, while a larger pericenter resulted in a comparatively longer tidal tail as the tidal forces act on the galaxy for a longer duration (Fig 3.8). Furthermore, a longer pericenter passage also resulted in a weaker

distortion of 7320c that is close to what is observed, due to less violent interaction as compared to a shorter pericenter passage.

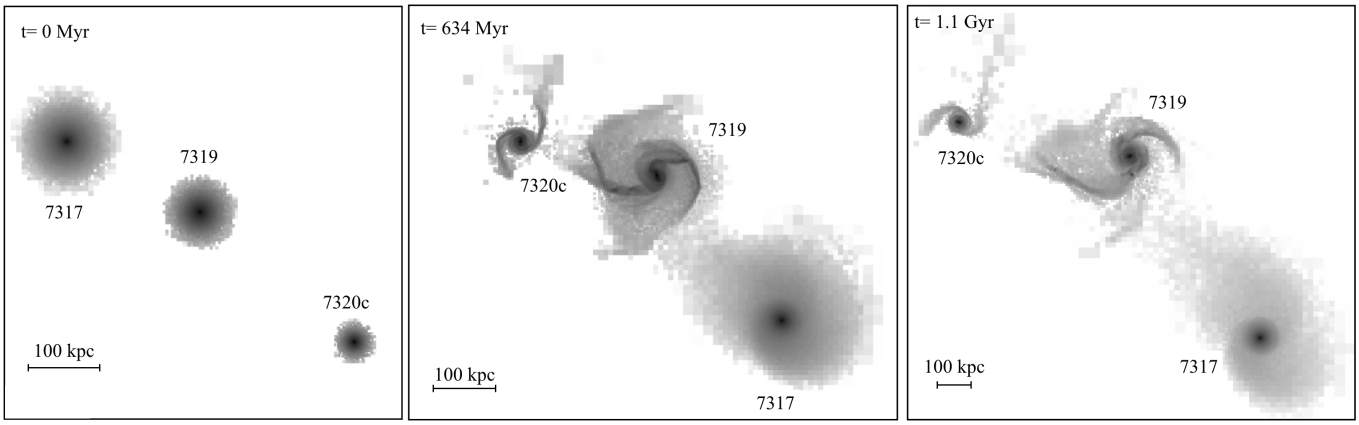

FIGURE 3.7: Shorter tidal tail resulting from a shorter pericenter (30kpc).

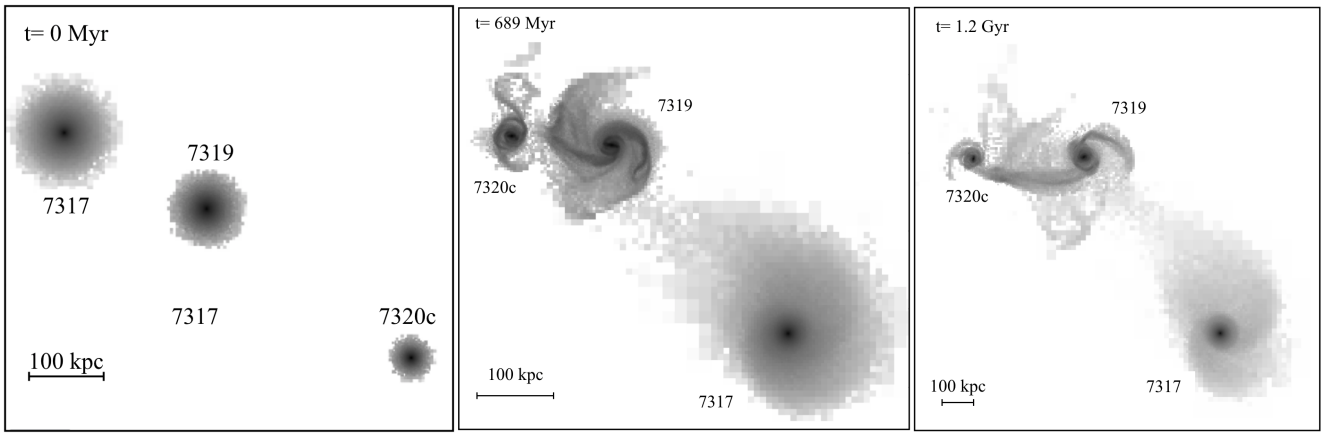

FIGURE 3.8: Longer tidal tail resulting from a longer pericenter (50kpc).

The galaxies until this point have orbital planes coinciding with the plane of sky, but for 7318a's interaction with the main galaxy, an inclined prograde orbit is required to avoid destruction of the formed in-plane outer tail. Such an orbit with an inclination of $\sim -25^{o}$ is found to yield a sharp tail resembling the observed inner tail (Fig 3.9). Finally, addition of 7318b is relatively simple, as it only interacts with 7318a from behind with a radial velocity of $\sim$ 900km/s with respect to the other members. The motivation behind modeling the Quintet in addition to obtaining the observed morphology, is to better explain hydrodynamics related features such as the HI maps and the shock wave. Although I observe a tail emerging from the 7319, the model doesn't find the mismatch in the gas and the stellar tidal tails as noticed in Williams et al. (2002). Moreover, although 7319 is deprived of majority of its gas, 7318a and 7318b still retain their gas content as opposed to the observed distribution of gas content of galaxies outside them. This probably implies that much stronger interactions are required to strip the gas from these galaxies. Furthermore, to obtain the shock as observed in Fig 3.1, I initially attempt a simple radial motion of 7318b and also an additional component of motion in the x-component directed towards the main galaxy to induce a compression in the inter-galactic debris. However, neither of these orbital configurations resulted in the desired shock possibly due to large separation between the main galaxy and the 7318 a & b pair and the intergalactic medium being too diffuse to be shocked. Yet, the interaction between the main galaxy and 7318a yielded a bridge like feature as noticed in Fig 3.10. The observations of the Quintet have revealed such a gas bridge between the main shock and 7318b (Cluver et al., 2010) in

addition to the main shock which could be of a different origin than the latter. A note is that, the feature in the gas map resembling the main shock is also a result from the same interaction and not to be misinterpreted as the shock from the intruder, 7318b with the intergalactic medium.

After the exploration of parameter space through ≈ 300 simulations (by varying galaxy masses, relative velocities, orbital eccentricities, pericenter passages and galaxy spin directions), although some of the features have been reproduced reasonably well (comparing Figs 3.3 & 3.11), my Quintet model does not yield all the features observed across a wide range of wavelengths. However, since this project is primarily focused at understanding the physics of starbursts in repeated interactions with Stephan's Quintet simply being one of the widely studied specimen, it is equally promising to model a general compact galaxy group that provides better control over the parameter space and also more spatially and temporally compact configuration as compared to the Quintet.

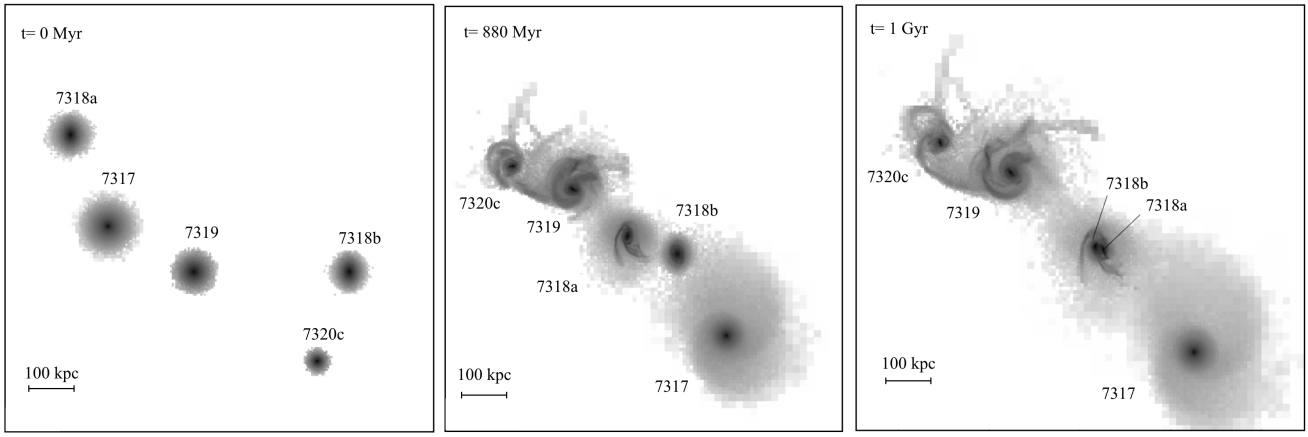

FIGURE 3.9: Final model with inner tail formation from the interaction of 7318a with 7319 in addition to the observed off-centered diffuse halo and the fainter outer tail.

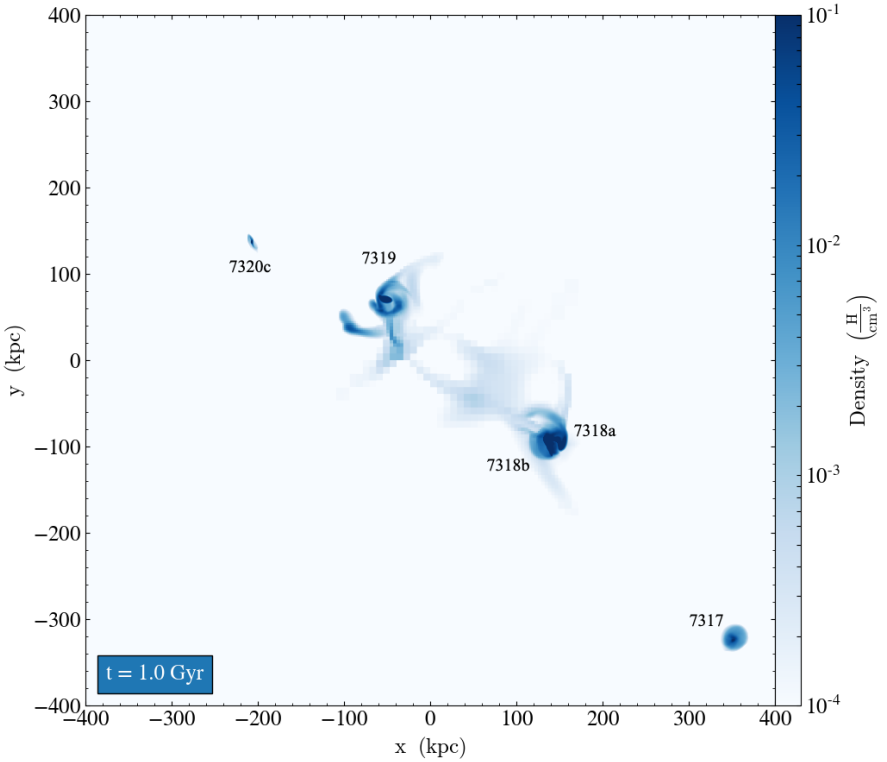

FIGURE 3.10: Gas density map of the Quintet from the final model with a shock.

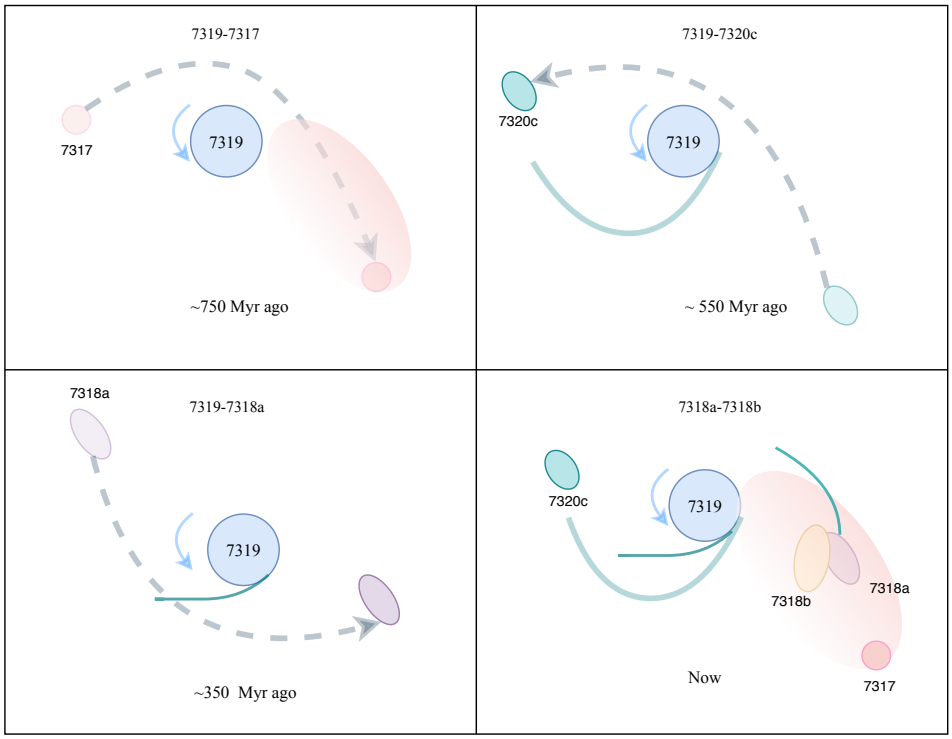

FIGURE 3.11: Final model formation scenario of the quintet after exploration of the parameter space showing the optical features that were reproducible. The model also places a constraint on the possible occurrence of the first interaction.

3.3 General compact galaxy group

Hereafter, I consider repeated interactions of 3 galaxies (two spirals and one elliptical), the model (see 3.12) and orbital parameters for which are tabulated in the appendix.

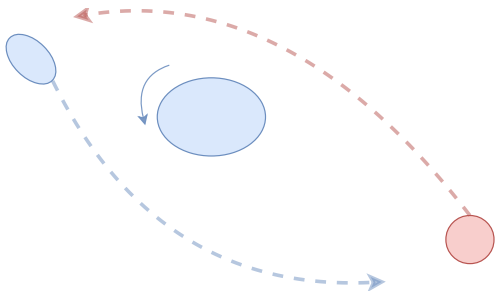

FIGURE 3.12: Model for interactions in a compact galaxy group. The galaxies in blue are the spirals and the other is an elliptical. The spiral galaxy in the center will be referred to as the main galaxy hereafter.

The system is modeled such that the duration between the interactions is less than the typical timescale galaxies take to resume their normal star forming mode after experiencing a starburst. The first interaction of the main galaxy is with the spiral and the pericenter passage occurs at closest approach of 17.6 kpc and the second interaction is with the elliptical and takes place $\sim$ 40 Myr later, with a pericenter approach of $\sim$ 23.6 kpc (Fig 3.13). Such a compact configuration is a reasonable imitation of a compact galaxy group and can allow us to probe the physics of star

formation in rapid repeated interactions. I first look at the factors contributing to the observed star formation for the total system first and then decompose the effect of individual interactions.

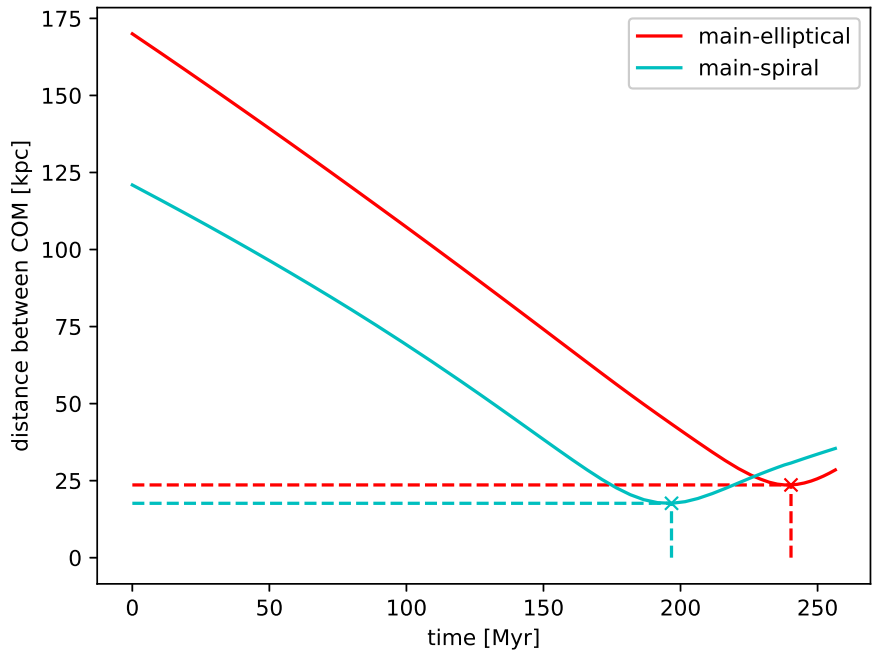

FIGURE 3.13: Distance between centers of masses of the perturbing galaxies with respect to time. The galaxy in the center is a spiral and would be addressed as the main galaxy and the galaxies marked in blue and red are the spiral and elliptical respectively. t=0 marks the beginning of the simulation.

Fig 3.14 shows the density projections of the interacting galaxies. With a smooth density distribution prior to the interaction, overdensities develop in the tails and central regions of the galaxies (main in particular) as the interaction progresses.

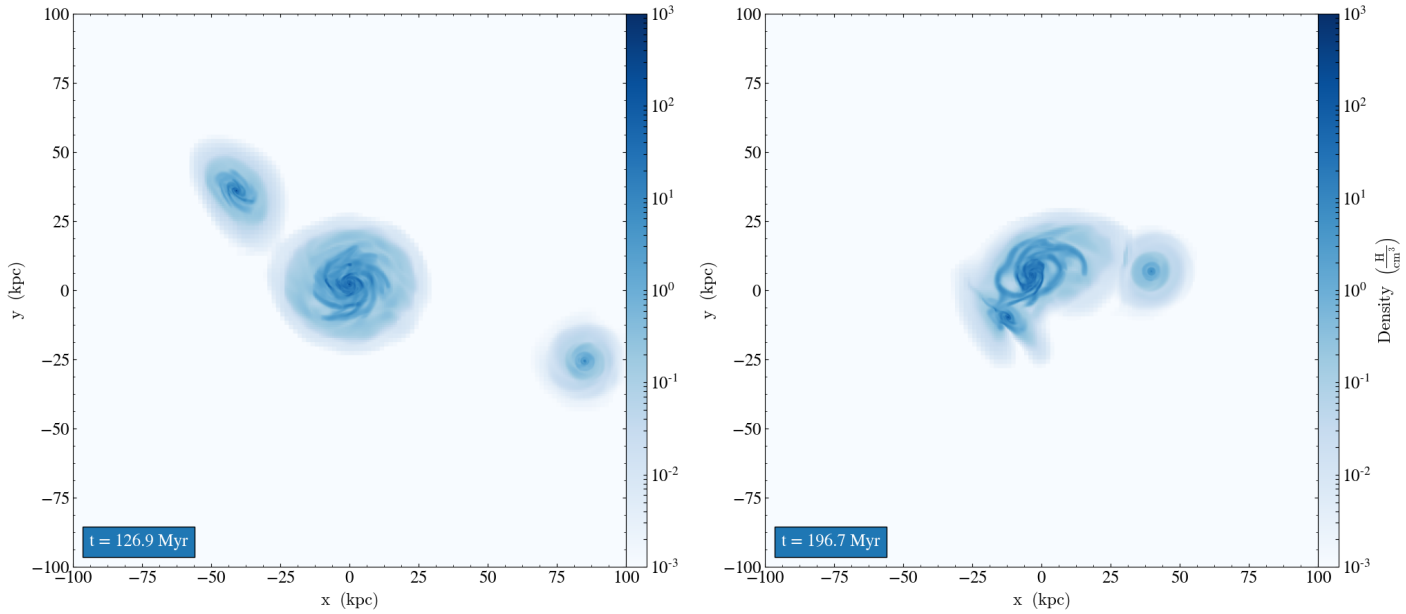

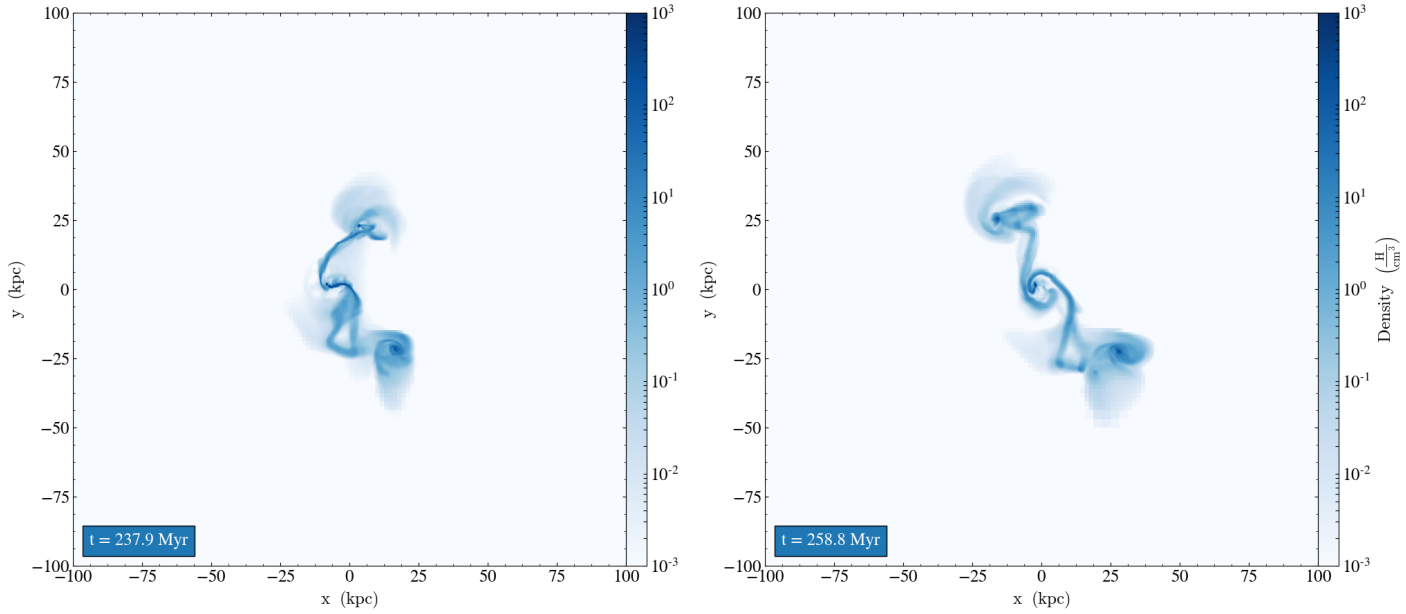

FIGURE 3.14: Density maps of the group prior to the interaction, after first and second pericenter passages and finally post interactions. The colorbar marks density in H/cm^3 ($H=10^{-24}g$)

Fig 3.15 shows the total star formation rate of the group. Intense starbursts are observed few tens of Myr after first and second pericenter passages. The SFR boosts from $\sim 5M_\odot/yr$ before the interaction to $\sim 500M_\odot/yr$ after the first pericenter passage. The SFR even goes higher by ~ 1.5 times after the second pericenter passage. The delay of $\sim$30 Myr in the burst after first pericenter passage could be attributed to the time taken for the gas to get dense enough for triggering star formation. However, since the second interaction is immediate and the gas is already brought to a dense state, such a delay is not observed in the second case where the starburst immediately follows the pericenter passage (dashed red line in Fig 3.15). Since star formation is related to the amount of gas at high densities, the distribution of gas in different density regimes during the course of interaction can provide a useful explanation for the observed SFR. Fig 3.16 shows density probability distribution functions at three different times: first pericenter passage (blue), post first (orange) and post second (green) pericenter passages (corresponding times marked with black dashed lines in Fig 3.15).

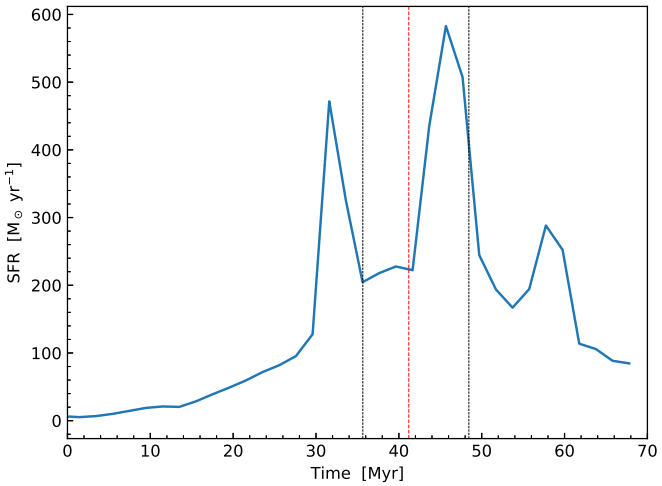

FIGURE 3.15: Total star formation rate of the group. t=0 in this and all the subsequent figures corresponds to the time of first pericenter passage and the red vertical dashed line marks the time of second pericenter passage. The dashed lines in black correspond to the times when density PDF profiles are computed (orange and green from Fig 3.16).

As expected, the PDF initially has a log-normal shape (e.g., Berkhuijsen and Fletcher 2008 ; Bournaud et al. 2010). Later, I observe a clear increase in the fraction of gas mass at high densities (> 50H/cc) after the first and even more after the second interactions, indicating gas being compressed to higher densities to facilitate intense star formation. It is worth reminding that this increase in dense gas could only be a partial contribution to the corresponding SFR enhancement by two-fold (with respect to the black dashed lines in Fig 3.15) since the adopted star formation recipe includes the fraction of H_2 as well contributing to the SFR (see equation 2.3). The truncation of the PDFs at high density however, is due to resolution limitation.

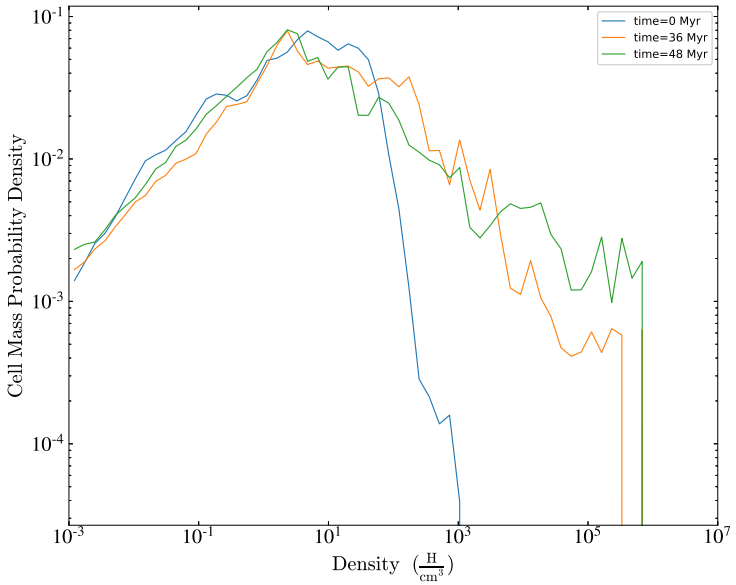

FIGURE 3.16: Evolution of density PDF over different times during the interaction. The PDF is computed considering the entire simulation box (400 x 400 kpc) and at maximum resolution.

Now that enhanced star formation is observed in interactions, I next look at the locations of these starbursts. Fig 3.17 shows SFR fraction in the central kpc and within 5 kpc of the main galaxy with respect to the total SFR. The plot depicts extended star formation (within 5 kpc) post first interaction (i.e., t=0), however, becomes more centrally concentrated (within central kpc) thereafter. This could possibly be because of the asymmetric distribution of gas by the interactions driving gas flow towards the center. The availability of gas in these regions (dense gas in particular) along the course of interaction can provide more elucidation on this observed SFR fraction. To compute such information, I plot the mass fractions of total gas as well as the dense gas (ratio of gas mass within a certain radius to total gas mass of the group) in these central and extended regions (the first and second panels from Fig 3.18).

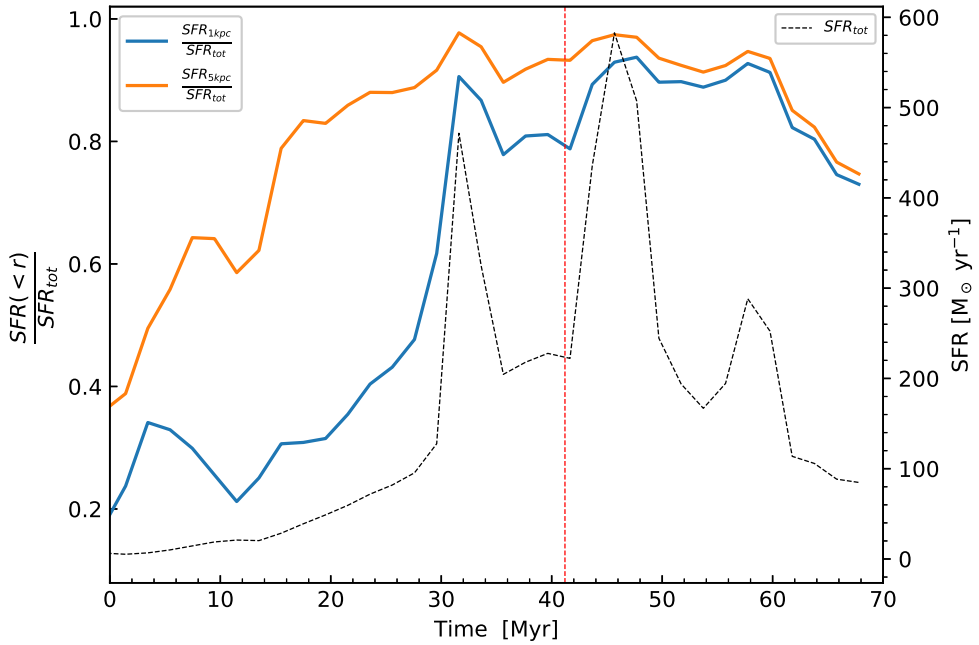

FIGURE 3.17: Central SFR (1kpc) and extended SFR (5kpc) with respect to the SFR of the entire group. The plot includes the total star formation rate as well (black dashed curve).

Within the central kpc, I notice an increase in the fraction of available as well as dense gas mass prior to the first and third starburst peaks indicative of gas inflows in this region contributing to the corresponding enhancement in SFR. However, with respect to the extended region, despite a significant enhancement in the dense gas fraction, this does not seem to contribute to the starbursts as the star formation is mostly in the central 1 kpc at the of this enhancement ($\sim$ t=30 Myr to t=45 Myr in the second and bottom panels of Fig 3.18). This could either be due to the feedback from the stars dispersing the dense gas before it could collapse into stars or that part of the dense gas has been stripped off as tidal tails beyond 5 kpc (see Fig 3.19), while the rest of it has migrated towards the central 1 kpc fueling nuclear starburst which also explains the SFR fraction initially high within 5 kpc, being dominated by central 1 kpc as the interactions progress. With respect to the second starburst peak, I observe an enhanced SFR despite no significant increase in the corresponding dense gas fraction in the central kpc which (as we will see later in a Kenicutt-Schmidt plot 3.27) could probably mean that the galaxy is forming stars more efficiently for a given amount of gas.

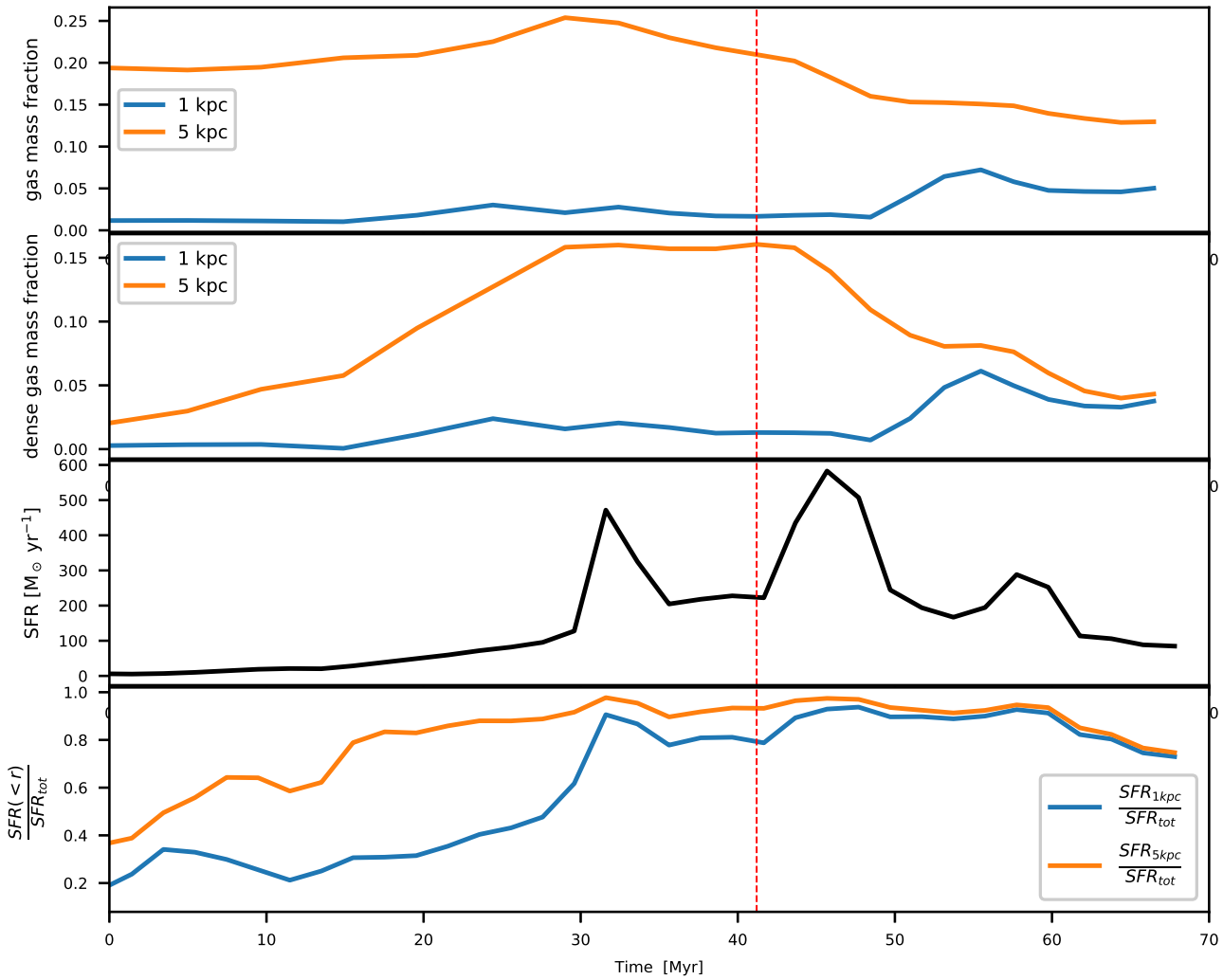

FIGURE 3.18: panel-1 (top): gas mass fraction in the central kpc and 5 kpc regions of the main galaxy; panel-2: mass fraction of dense gas ($\rho > 50$ H/cm^3) in the central kpc and 5 kpc regions of the main galaxy ; panel-3: total SFR of the group ; panel-4: fractions of SFR in 5kpc and central kpc around the main galaxy.

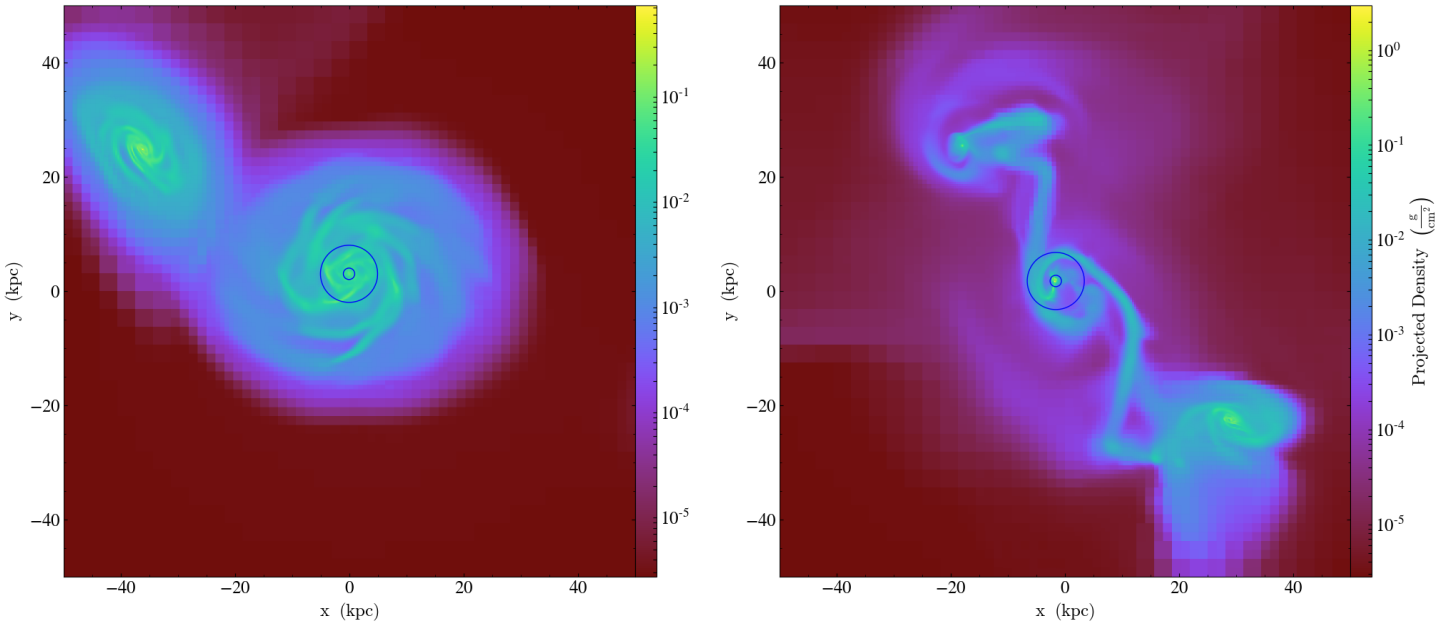

FIGURE 3.19: Zoomed-in projected density images of central kpc and 5 kpc of the main spiral as the interactions progress. The circles represent central kpc and 5 kpc of the main spiral. Formation of tidal tails leaves empty space within 5 kpc empty which explains insignificant SFR contribution from the region 1 kpc < r < 5 kpc

Higher velocity dispersion in the gas can favour star formation through increased turbulence and cloud collisions. Since interactions can stir up the gas increasing this dispersion (e.g., Powell et al. 2013), looking at how this quantity varies in our simulation can provide further insights into understanding the observed SFR. The velocity dispersion of gas, however, can also be increased due to feedback from the star formation and its exact origin is therefore obscure. To assess its role on star formation, the velocity dispersion needs to be computed over scales of GMCs. I compute a 3D velocity dispersion over a scale of $\sim$ 80pc that is then mass-weighted averaged over a cube of 20 kpc around the main galaxy's center. The region is selected so as to include almost the entire disc of main galaxy and also to not allow significant inclusions of the other two galaxies during the interactions. Fig 3.20 shows a clear correlation between the peaks of star formation and the velocity dispersion where the velocity dispersion is enhanced by almost a factor of 8 with respect to the pre-interaction value. This indicates that interactions enhance turbulence that is reflected in the enhancement in the gas velocity dispersion. This enhanced dispersion in turn is contributing to the observed starbursts.

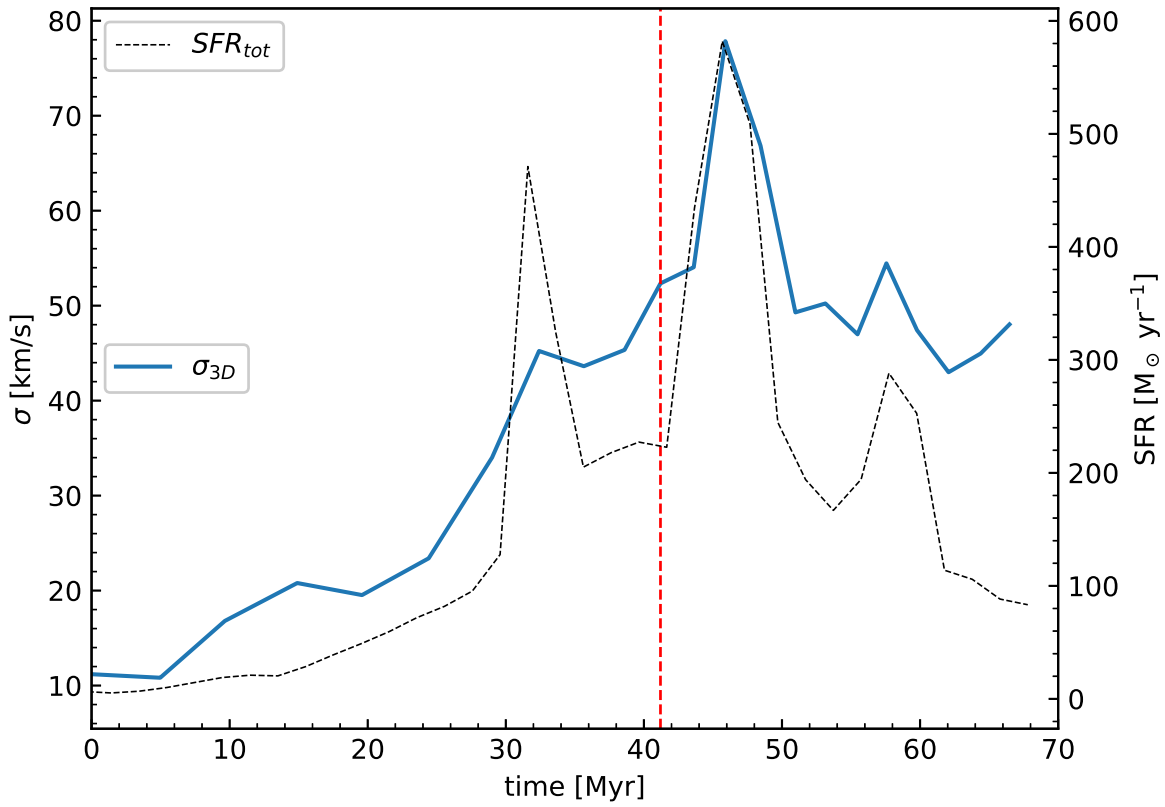

FIGURE 3.20: 3D velocity dispersion of gas in a box enclosing volume 20 x 20 x 20 kpc^3 around center the main galaxy overplotted with the total SFR (black dashed curve).

A measure of star forming efficiency in a galaxy is how fast it depletes its gaseous component at its current SFR. Fig 3.21 shows the depletion time ($\frac{M_{gas}}{SFR}$) for the main galaxy considering a 20kpc region around its center. At the highest SFR, the depletion time of the galaxy is $\sim$ 25 Myr, similar to that of starburst galaxies like Ultraluminous Infrared Galaxies (Daddi et al., 2010b) and the depletion times with respect to the starburst peaks remain fairly constant despite different SFRs. This can be attributed to the galaxy forming stars at a high and almost constant efficiency in the starburst mode and also the gas mass depleting along with dropping SFR (corresponding to the third SFR peak).

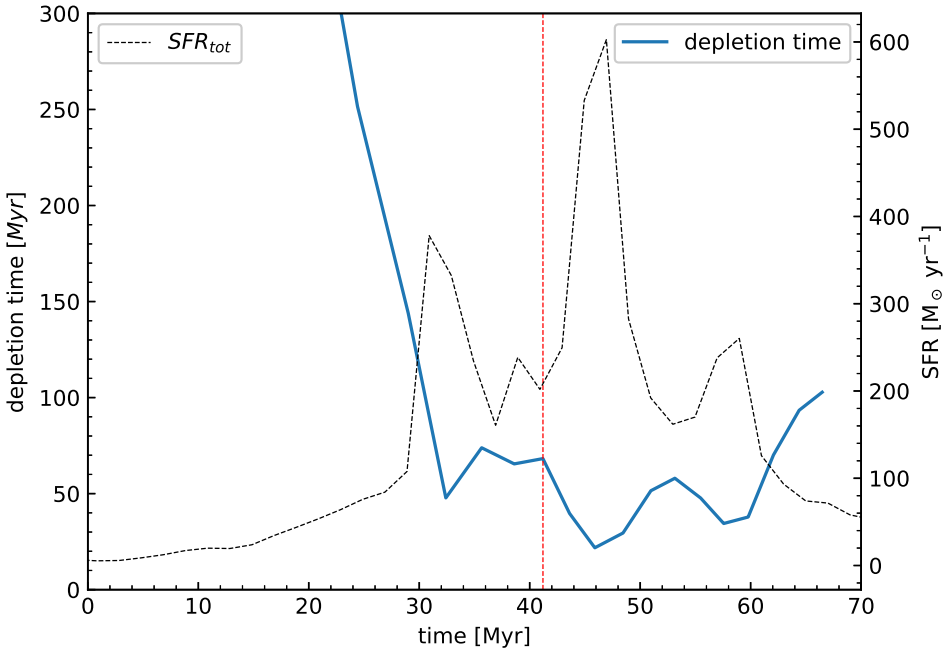

FIGURE 3.21: Depletion time of the main galaxy overplotted with total SFR (black dashed curve). The vertical dashed line corresponds to the second pericenter passage.

To evaluate the effect of individual interactions, I decompose the combined interaction between three galaxies into discrete encounters by modeling the first encounter (main-spiral). In this case, such a decomposition additionally will shed light on the effect of the missing second interaction as well (main-elliptical). The individual interaction of main-spiral is modelled such that approximately same effect as that of the first interaction in the three galaxies case is achieved (i.e a similar pericenter distance ($\pm$ 1 kpc) and the velocity of the encounter ($\pm$ 50 km/s at the pericenter). To do so, the original orbital parameters (positions and velocities) of the main and spiral galaxies are to be adjusted accordingly to compensate for the missing gravitational effect from the elliptical. Fig 3.22 shows the SFR of the individual interaction and the combined interactions (main-spiral-elliptical) with t=0 marking the time of pericenter passage in main-spiral interaction that is adjusted to coincide with the time of first pericenter passage in the combined case. From the figure, it can be noticed that the SFR in the main-spiral interaction begins to peak $\sim$ 10 Myr after the onset of first peak in the case of combined interactions. Furthermore, the enhancement in SFR in the former case is lower as compared to the enhancement observed in the latter case implying that the second interaction with the elliptical galaxy is not only triggering an early onset of starburst but also enhancing the intensity of star formation. Fig 3.23 shows contribution to the enhancement in SFR from main-spiral interaction and the plot is the ratio of the SFR of the entire group to the SFR of main-spiral interaction. Without the elliptical, the contribution of main-spiral interaction to the starburst peaks of the combined SFR is $\sim$ 14%, 25% and 50%.

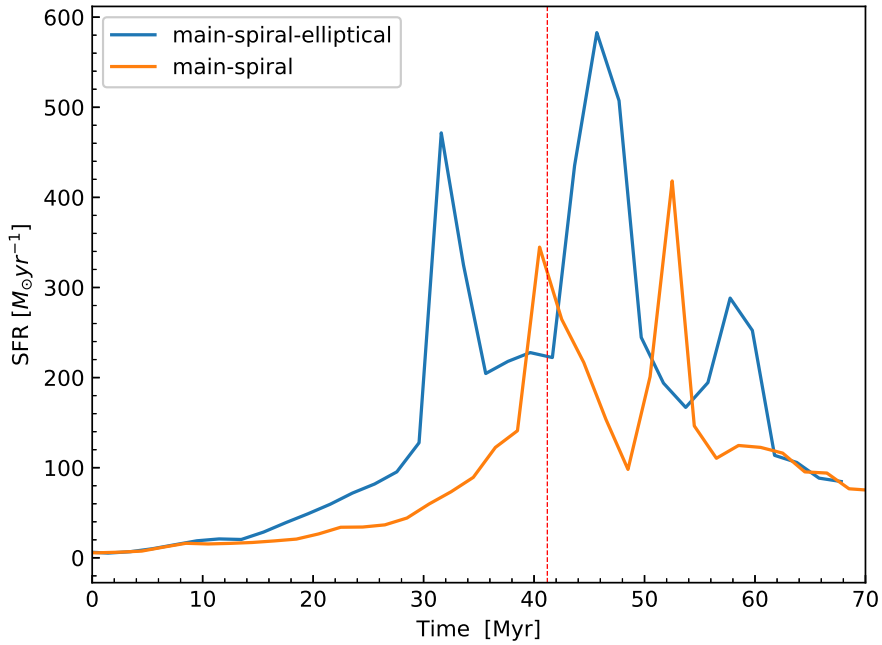

FIGURE 3.22: SFR in spiral-spiral interaction overplotted with SFR from the 3 galaxy case. t=0 marks the time of pericenter passage in the main-spiral interaction (coincides with the time of the first pericenter passage in main-spiral-elliptical).

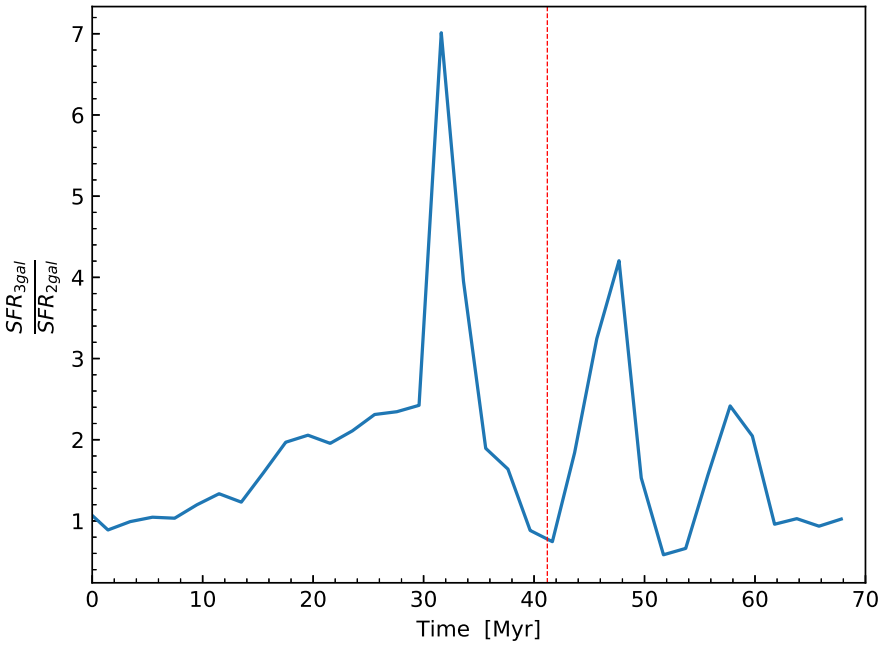

FIGURE 3.23: Comparison of SFRs in the cases of main-spiral-elliptical and main-spiral interactions through ratio of SFRs. Considered SFR of main-spiral is obtained by interpolating the actual SFR to the time points corresponding to the SFR of main-spiral-elliptical.

So far, a boost in the starburst has been observed with the current configuration of compact galaxy group. However, to verify if this scenario is a representative of other general compact galaxy groups, or if the other two star formation scenarios: saturation and quenching are possible as well, I explore three other different orbital configurations of the considered compact galaxy group.

3.4 Orbital configurations of compact galaxy group

Since, we notice that the the former configuration leads to a strong interaction, where the main galactic disc is truncated during the course of interaction, these new orbital configurations are such that the interactions are less extreme and the majority of the main galaxy's disc is retained. These configurations (see Fig 3.24) are:
(A) The original configuration: A prograde encounter of the main galaxy with respect to the other spiral and elliptical galaxies.
(B) A retrograde encounter of the main galaxy with respect to both the elliptical and the other spiral while keeping the pericenter passages and time duration between the interactions almost constant as in the case of initial configuration.
(C) A prograde encounter of the main galaxy with an increased pericenter passages by ≈ 8 kpc (with the spiral) and ≈ 13 kpc (with the elliptical) while keeping the time between the interactions nearly unchanged.
(D) Inclined orbits of the spiral and the elliptical galaxies by $\approx 30^{o}$ while the pericenter passages and the time gap between interactions remains same as the initial configuration.

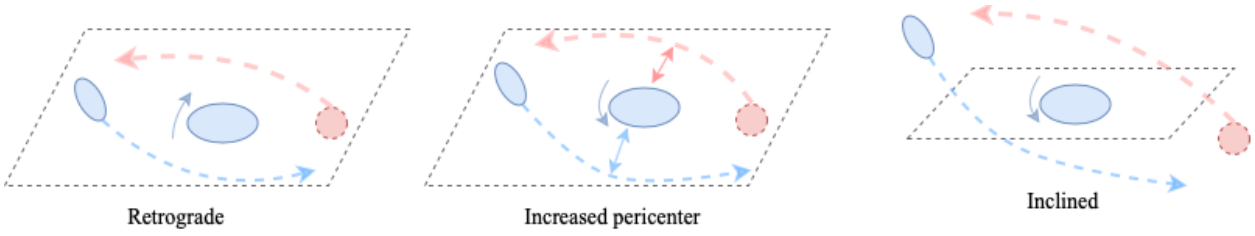

FIGURE 3.24: Less extreme orbital configurations of the compact galaxy group. The galaxy types and their physical parameters are the same as in the original configuration. The dashed rectangle represents the plane of the main galaxy

Fig 3.25 shows the SFR for all the three configurations and we immediately notice no saturation or quenching effect despite the group's configuration being less extreme than the original configuration. With respect to the locations of the observed starbursts, while the configurations of retrograde and inclined orbit encounters follow a similar trend as that of the original configuration where the starburst peaks correspond to the central regions due to gas inflows, the increased pericenter leads to a spatially extended star formation during the burst before star formation becomes centralized at the later stage (see Fig 3.26). This can be attributed to the decrease in tidal torques (inversely proportional to the distance between galaxies) which are responsible for driving gas flows towards the galactic nucleus.

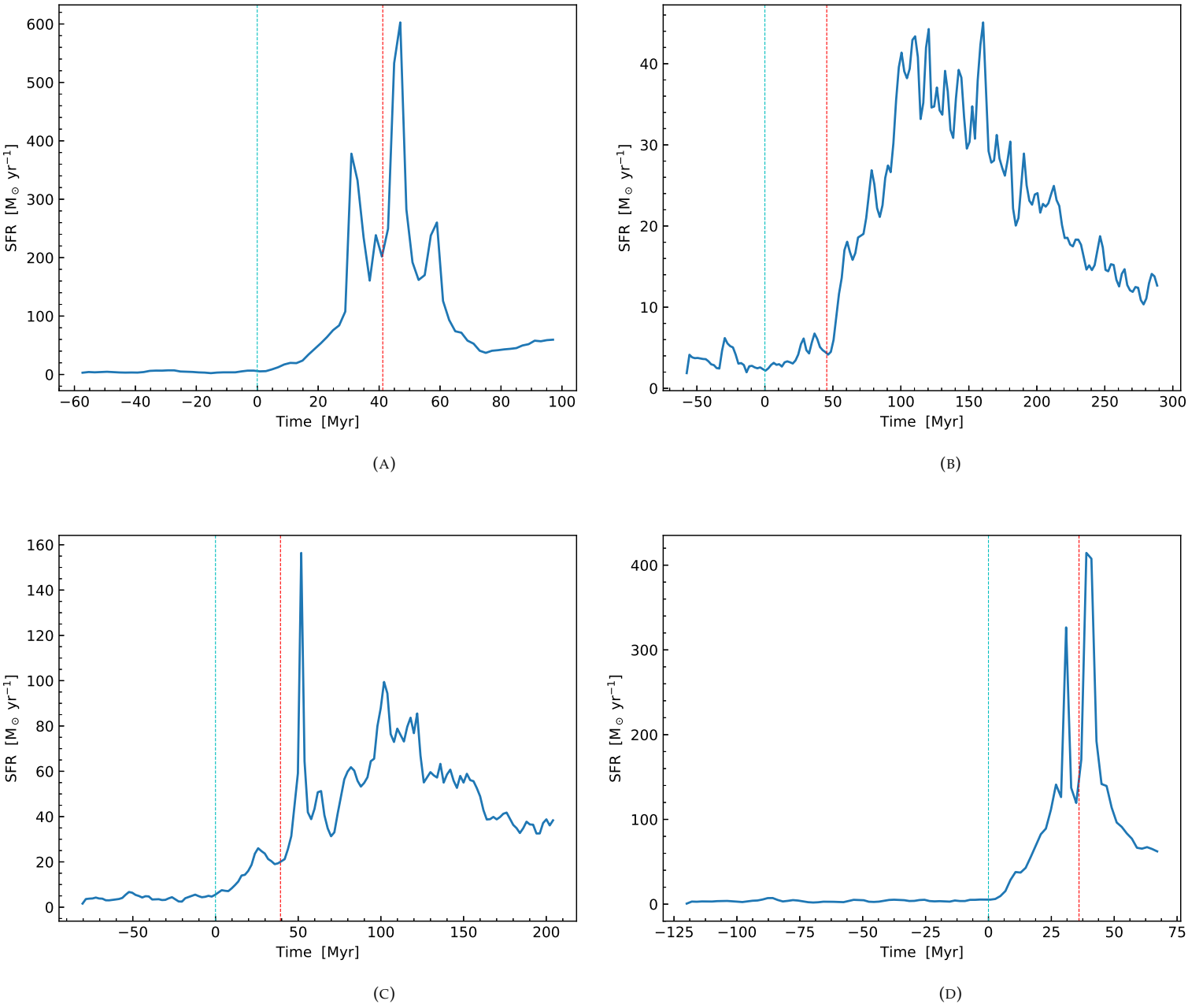

FIGURE 3.25: Total SFR of the groups (A - prograde ; B - retrograde ; C - increased pericenter ; D - inclined orbits) where the dashed lines represent the first and second pericenter passages.

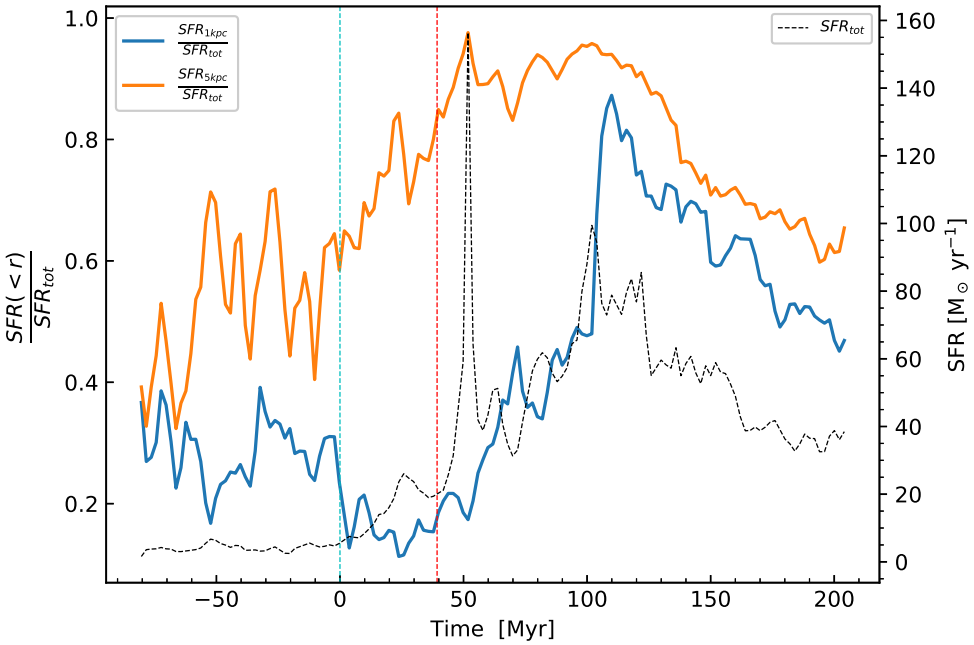

FIGURE 3.26: Ratio of star formation rates in 5kpc and central kpc around the main galaxy to total SFR of the group in the case of increased pericenter distances.

One of the key insights into understanding the galaxy evolution is how star formation in galaxies relates to the physical conditions of the interstellar medium and the Kennicutt-Schmidt diagram (linking surface densities of gas and SFR) is one of the widely adopted diagnostics to evaluate how efficient different galaxies are in converting their gas to stars. Fig 3.27 shows the relation between surface densities of SFR and the amount of total gas in an area of 20 x 20 kpc^2 around the main galaxy's center. The dashed lines approximately follow the disc (bottom) and starburst (top) sequences in Daddi et al. (2010a) representing approximately constant depletion times of ≈ 1 and 0.1 Gyr respectively and the markers representing pericenter passages. I observe that prior to the interaction and even at the first pericenter passages, the galaxies are in normal disc galaxy regime with depletion times of few Gyr (see Fig 3.28). However, after the first pericenter passage, the main galaxy proceeds to starburst mode with corresponding plummet in depletion times. In Fig 3.28, I note about an order of magnitude drop in this time of depletion from the pre-interaction phase to the starburst. But, the latter configurations being weaker than the prograde configuration, they do not exhibit as strong drops in their depletion times as in the case of prograde which is also reflected in their SFRs (Fig 3.25). Had the scenario been quenching or saturation, I would have expected the depletion time to rise (sharply in case of quenching due to sudden drop in the SFR) after the interactions, but instead, I only notice a modest rise in all the configurations due to boosts in the starburst. I also note that despite the star formation returning to a quiescent value (i.e almost that of pre-interaction phase), the galaxy still remains in the starburst phase until the end of simulations rather than falling back to disc regime. This indicates that the star formation persists to be efficient and the exact explanations for this increased efficiency are still being studied. Possible explanations could be the modification in the star formation mechanism itself (Renaud et al., 2019) and the type of galaxy interactions such as the prograde and retrograde encounters (as noticed in our Kennicutt-Schmidt plot).

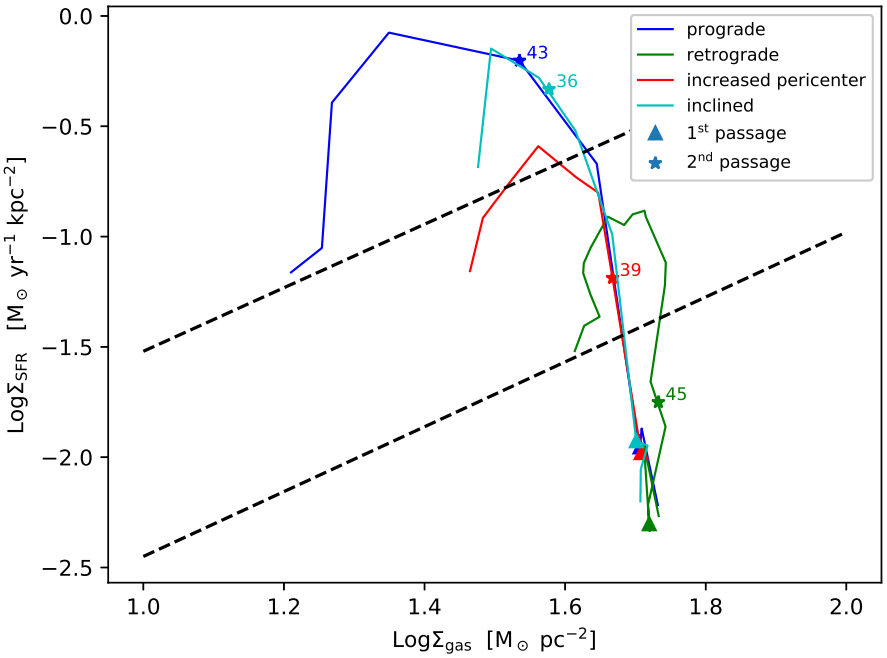

FIGURE 3.27: Kennicutt-Schmidt plot of the main galaxy in all the configurations (including the original: prograde) where the dashed lines represent normal disc regime and starburst modes from Daddi et al. (2010a). The triangle markers represent first pericenter passages. The stars indicate second pericenter passages (with times indicated with reference to the first pericenter passages in Myr).

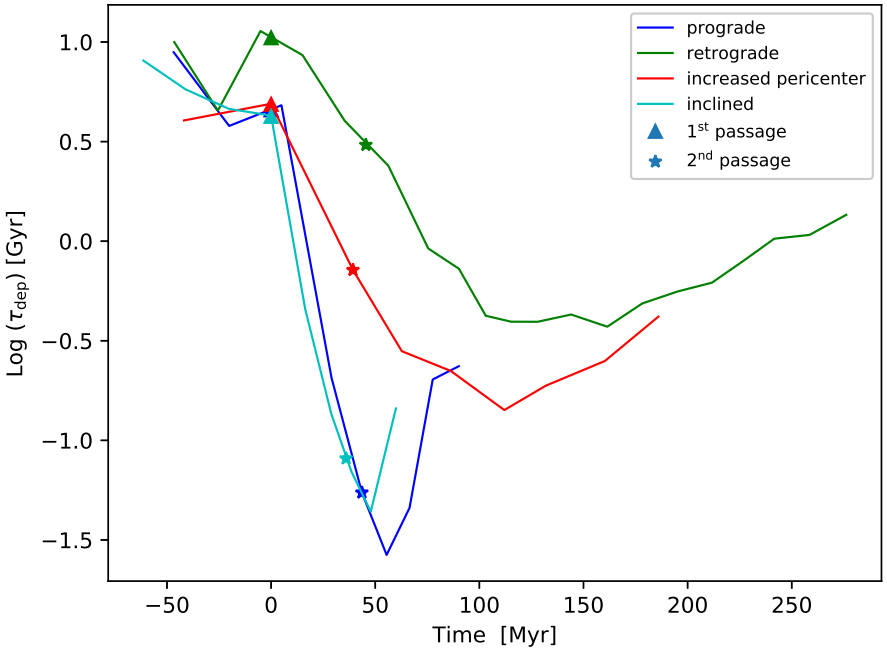

FIGURE 3.28: Depletion time of the main galaxy during the course of interaction in all the configurations (including the original: prograde). The triangle and star markers are same as in the Fig 3.27

Like I previously noted the increased gas velocity dispersion contributing to the observed starburst peaks in case of prograde configuration, I now check if this is followed in other configurations as well. I note a similar trend of interactions driving the velocity dispersion in gas contributing to the starbursts (see Fig 3.29). Although the velocity dispersion closely follows the SFR during the initial stage of the interaction, it diverges from SFR post interaction where the velocity dispersion peaks do not fallback to their initial values and this could be one of the reasons why the starburst galaxy continues to form stars efficiently. Possible explanations for such a behaviour of the gas velocity dispersion could be attributed to feedback from the stars formed during the bursts, and/or net inflows of gas from the inter-galactic medium and tidal debris into the galaxy maintaining it high.

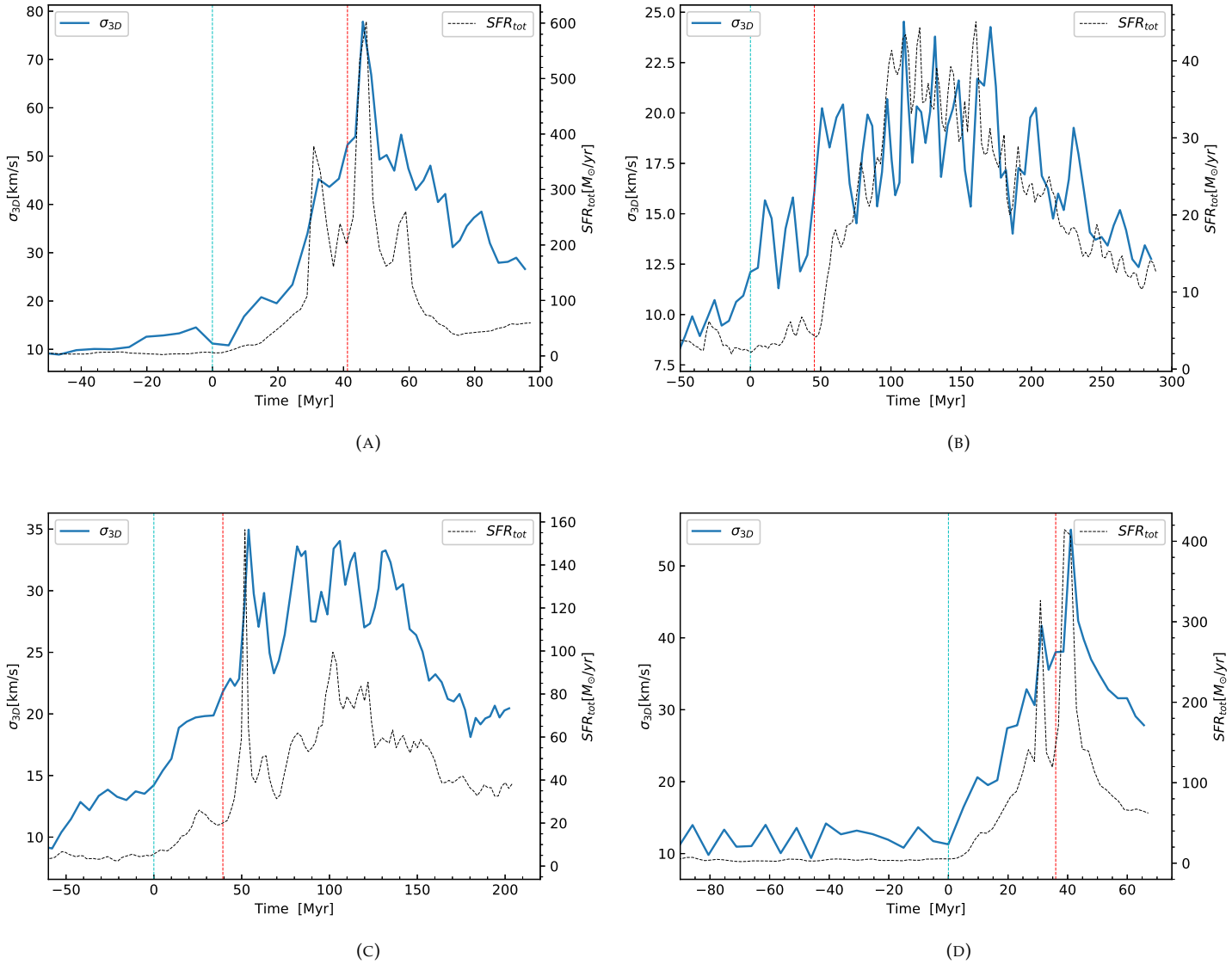

FIGURE 3.29: 3D gas velocity dispersion of main galaxy (20 kpc around the galaxy center) (A - prograde ; B - retrograde ; C - increased pericenter ; D - inclined orbits) where the dashed lines represent the respective first and second pericenter passages.

I move ahead with exploring the latter possibility. The rate of depletion of gas mass of the galaxy accounts for the combination of star formation rate, gas inflows, outflows and feedback. To verify if the net gas inflow (inflows-outflows) into the galaxy is contributing to the observed velocity

dispersion pattern, it can be approximated to be the rate of depletion of gas mass added to the corresponding SFR (the total SFR of the group is considered here since SFRs of the other two galaxies are negligible as compared to that of the main galaxy), while feedback is neglected for simplicity. Fig 3.30 shows the net inflows through a boundary of 20kpc around the main galaxy's center in different orbital configurations. From the plots, the relation between inflows and velocity dispersion appears to be cyclic where, although inflows initially seem to enhance the velocity dispersion, this enhancement is momentarily regulating the inflows likely because of feedback-driven galactic outflows and the velocity dispersion is enhanced again. But, we do observe a positive inflow of $\approx 50 M_{\odot}/yr$ post interaction phase where the velocity dispersion is diverging from the SFR in all the configurations.

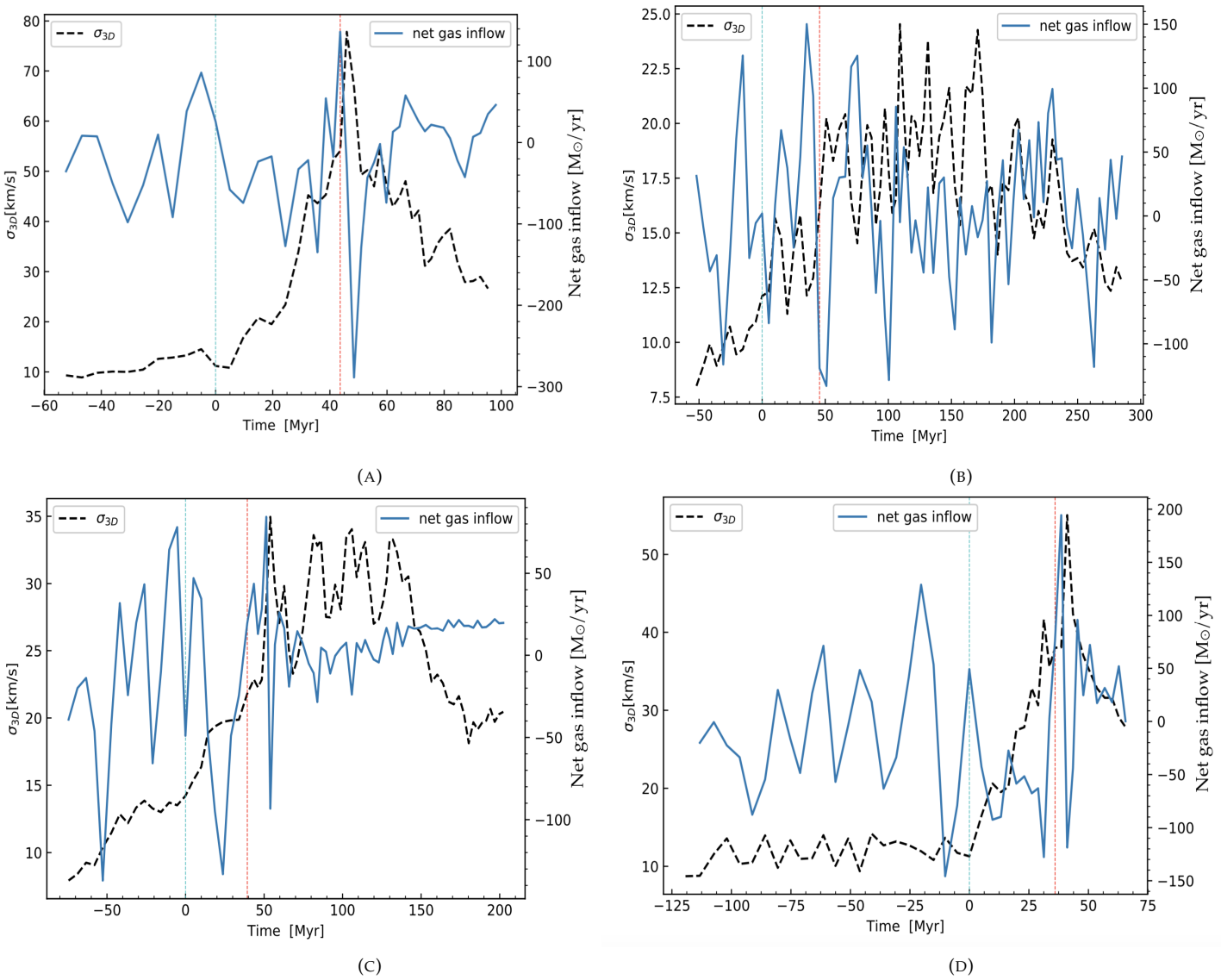

FIGURE 3.30: Net gas inflow rate computed over 20 kpc around the galaxy center overplotted with the velocity dispersion (black) (A - prograde ; B - retrograde ; C - increased pericenter ; D - inclined orbits) where the coloured dashed lines represent the respective first and second pericenter passages.

The effect of stellar feedback, however, is not straightforward to implement. With continuously transforming interstellar medium during the interactions, it is extremely complex to capture how the supernovae explosions propagate and compute the time delays when they begin to significantly contribute to exciting the gas and thereby the velocity dispersion.

So far, we have seen that the repeated interactions in our compact galaxy group configurations led to boost in starbursts mainly contributed by tidal torques triggering nuclear gas flows and interactions enhancing the gas velocity dispersion. However, whether these configurations are representative of all the compact groups in reality and what missing physics in the models would make them more realistic is discussed in the following section.

Chapter 4

DISCUSSION

4.1 Stephan's Quintet

The model discussed in this report for the formation scenario of the quintet is not a unique solution. Previously proposed scenarios derived from a N-body simulation (Renaud et al., 2010) which was able to reproduce the stellar morphology of the Quintet but not any hydrodynamical features such as the shockwave. Extending the N-body simulations and including hydrodynamics, Hwang (2010) explains the some of the gas features and the group's kinematics relatively well, although it still remains unaccountable for the galaxies retaining their gas and the starburst locations. Considering the role of the elliptical member, 7317 obtained from recent observations, kinematics of the members and the ages of stellar clusters in tidal features, the proposed model in this report is another possible idea for the Quintet's formation. While the stellar features have been reproduced reasonably well with the model, the shock wave resulting from the high speed intruder is still irreproducible. However, I observe a gas bridge between 7319 and 7318b formed from the interaction between 7319 and 7318a, a feature also noticed in the SPH simulations of the same encounter (Hwang et al., 2012). Furthermore, including star formation models can help better constraint the formation scenario, however our current model does not incorporate one yet in order to be able to compare with the observed starburst features. This shows the complexity in constructing a single hypothesis to constrain all the observed features in a compact galaxy group that only escalates with the increasing number of galaxy members. Stephan's Quintet proves to be an informative example of a compact galaxy group due to its remarkable features from interactions and such kind of interactions are a frequent phenomena in other compact galaxy groups as well at some point in their evolution histories. The exploration of parameter space put forth in this report can be applicable even to a general compact galaxy group in understanding the relation between certain orbital parameters and the kind of features they yield. While numerical simulations can span a limited range of compact galaxy group environments, multi-wavelength observational surveys (e.g. Tzanavaris et al. 2010) are necessary to understand the physical processes in compact galaxy groups on a broader range. Deep optical observations using instruments such as the Canada-France-Hawaii Telescope (Duc et al., 2018) can be extremely useful in not just revealing the previously undetected features, but also in better constraining the interaction history of a group through numerical simulations. The complexity in modeling the quintet, and the proposed model yielding a relaxed configuration where compact galaxy groups typically are much more compact both spatially and temporally motivated us to model a simpler compact galaxy group to explore the physics of its star formation.

4.2 General compact galaxy group

- Active Galactic Nucleus:
  Since feedback is one of the crucial factors determining star formation, the feedback recipes employed can drastically change the observed star formation behaviour. Numerical simulations are limited by resolution where it is not feasible to accurately incorporate all the feedback contributors on wide range of scales. For instance, although our model takes into account stellar feedback, feedback from AGN is not included as we do not have precise subgrid models to incorporate the accretion effect onto the AGN. But, as pointed in the introduction, AGN feedback is crucial for the evolution of massive galaxies like the galaxies in our models. Since, we find enhancement in gas mass in the central region during interactions, AGN in such a situation could provide a strong feedback by feeding on this enhanced central gas content and driving powerful jets, thereby can be expected to yield a more regulated star formation than obtained in the central regions. Furthermore, strong AGN feedback is found to morphologically convert the disc galaxies into ellipticals (Dubois et al., 2013a) and the time at which this morphological transformation happens can be crucial in galaxy interactions. For instance, if the galaxy is morphologically quenched by AGN after the first interaction itself, we might not expect the observed boost in starburst during the subsequent interactions, but instead, a sudden halting of star formation could be expected. Not only can AGN affect the morphology of its host galaxy, the fate of the end product in galaxy interactions in a compact galaxy group can be highly dependent on AGN feedback as gas inflows become predominant at the coalescence stage, and without AGN, the merger remnant could still have cold gas reservoir to form stars. On the contrary, the presence of AGN can turn the merger remnant into a quenched galaxy as noted in simulations of a galaxy pair merger in Di Matteo et al. (2005). Observationally, the presence of AGN can also influence the way we interpret the starburst galaxies. Infrared emission is considered to be a tracer of star formation and Sanders and Mirabel (1985) have observed an increase in this emission for a sample of radio bright galaxies despite having equal amount of available gas as that of the MilkyWay (i.e a short depletion time). However, if an AGN embedded in dust could significantly contribute to the infrared emission (e.g: Telesco et al. 1984), this can reflect as an increased efficiency although the efficiency could be similar to that of disc galaxies. Incorporating AGN models in the simulations could therefore be useful in affirming if the enhanced efficiency in starburst galaxies is a result of the modified star formation physics or an observational misinterpretation. However, precise implementation of AGN feedback in interactions might not be straightforward as gas flows towards the center at different rates during the course of interactions and different accretion rates give rise to different modes of AGN. A simple way to incorporate a self-consistent AGN could then be to insert an initial seed and consider two phases of gas accretion that is dependent on local gas conditions (example of such a prescription: Bondi 1952): a low accretion mode prior to the interaction, injecting certain energy into the surrounding medium, and a high accretion mode injecting higher feedback energy into the medium due to increased gas inflows as the interactions progress (Sijacki et al., 2007). In addition, a black hole's spin can also influence the feedback to an extent through accretion efficiency. A black hole with a spin aligned with the galactic disc tends to accrete matter efficiently this translates into an efficient feedback, while non-rotating black holes and retrograde black holes provide less efficient feedback (Tchekhovskoy and McKinney, 2012).

  So far, we have been considering negative effects of AGN feedback on the observed star formation, if incorporated in our models. However, AGN can potentially have a positive effect on star formation as the AGN outflows compress low density gas in the extended disc regions and trigger star formation (Ishibashi and Fabian, 2012). In our models, this could correspond to the region of extended tidal tails emanating from the main galaxy and we

might expect an even more severe effect of such positive feedback during the interaction if either of the other two perturbing galaxies also possess an AGN.

- Magnetic fields: A potentially important source of non-thermal pressure acting against gravitational collapse of gas and is neglected for simplicity sake in our simulations is the effect from magnetic fields. While some of the early works found that magnetic field moderately regulated star formation in starburst regions (e.g., Van Loo et al. 2015), turbulence driven magnetic field is observed to hold a tight correlation with SFR density (Tabatabaei et al., 2013) where turbulence from SNe in star forming regions amplify magnetic fields (e.g., Balsara and Kim 2005) which could in turn act against the gas collapse and regulate star formation. In the case of interactions, turbulence driven magnetic fields could therefore be important especially at the central regions with gas inflows triggering intense starburst and in addition, with the inclusion of AGN, a complex interplay between this magnetic field and the AGN's magnetic field can be expected and the combined effect could then be dependent on if the AGN's field adds up to or attenuates the other. If the magnetic field is acting against formation of dense gas, we can as well expect this to be reflected in the analytical expression of probability distribution function of gas density (see equation 1.3). E.g., Molina et al. (2012) considers three different modes of how magnetic field is coupled to the gas and finds a decrease in the width of the Probability Density Function when magnetic field varies as a function of gas density (equation 1.3 represents unmagnetized case).

- Extrapolation to high redshifts (z):
A crucial parameter determining the strength and duration of starbursts is the gas content and its response in interacting galaxies and galaxy interactions in compact galaxy groups at low z can act as helpful local analogs in providing insights into interactions at higher redshifts (Sulentic, 2002). With the galaxies' gas fraction as low as $\approx 10\%$ (thus a good analogy for galaxies at low z), I notice an enhancement in the star formation rate by a factor of $\sim$ 100 and $\sim$ 120 during the first and second interactions respectively. However, galaxies in the past are known to be gas-rich ($\approx 50 - 60\%$) and to reside in much denser environments [3] where the interactions were frequent and more violent than today. Furthermore, the gas velocity dispersion in high f_{gas} galaxies at high z is also observed to be higher (e.g., Oliva-Altamirano et al. 2018) which is expected to be enhanced by interactions as observed in our results. Considering these, it is only intuitive to expect powerful starburst episodes in compact galaxy groups at higher z as compared to low z case. Studies (e.g., Di Matteo et al. 2008) modeling interactions at high z, have however revealed a surprising outcome. While low z interactions were found to enhance SF to moderate levels, high z interactions exhibited neither a significant enhancement in the star formation nor the starburst duration as compared to the local counterparts. Fensch et al. (2017) further investigated physical causes behind this peculiarity through comparison of interactions between high gas fraction, f_{gas} galaxies at high z with low f_{gas} galaxies ($\approx$ 10%) at z=0. Similar to the result obtained in this work, while gravitational torques induced strong gas inflows at the galactic nuclei for their low z galaxy interaction, with respect to interaction involving high f_{gas} galaxies, this became less significant as the pre-interaction gas inflows were as such stronger due to disk instabilities and the efforts of torques to further increase the inflows turned out less effective. In the extended disc region, a lower enhancement in the dispersion of gas (turbulence) during the interaction and difficulty in the gas compression due to their location inside the clumps has limited the ability to achieve relatively higher SFRs in high f_{gas}. This implies that the mechanism to fetch the galaxies to an excited state of high SFR (interactions in our model and high f_{gas} in Fensch et al. 2017) change the way how subsequent interactions affect SFR. Furthermore, if AGN is to be included in such a situation, its effect on these galaxies

[3] Due to universe itself being denser at those redshifts. $\rho_{matter} \propto (1+z)^3$

could be different from that of low f_{gas}. Since, high f_{gas} galaxies have saturated central inflows right from the beginning, AGN activity would also be stronger right from the initial stages of interactions possibly even regulating clump formation as observed in Dubois et al. (2013b). This accretion onto AGN would eventually saturate and might not trigger as intense star formation as in low f_{gas} galaxies at the coalescence stage leaving the remnant to be a potential disc galaxy still forming stars.

- The star formation scenario corresponding to a single compact galaxy group configuration cannot represent all possible conditions of compact galaxy groups. Modeling different configurations of various orbital and model parameters is a way to explore the possible star formation scenarios. In this report, since the initial configuration led to a boost in the starburst, I modelled the other compact groups to see if quenching or saturation is possible. As the former configuration is extreme in terms of SFR enhancement, the others are modelled to be weaker and is done so through three parameters: spin-orbit coupling (retrograde), wider pericenter passages and non-coplanar orbits of the galaxies, however, none of them yielded a different scenario. Since the parameters are modified exclusively (maintaining the other parameters to be almost the same when a specific parameter is modified), I do not expect changing combinations of the considered parameters to result in a different scenario. Therefore, one likely approach to observe a quenching or saturation scenario is to look for different model parameters of the galaxy members. This could include:
  - Increasing gas fraction of the galaxies in order to see a possible saturation (like in Fensch et al. 2017) since the gas velocity dispersion of the galaxy could saturate from already forming stars at its maximum rate.
  - Mass ratio of the interacting galaxies, where major mergers (involves galaxies of comparable masses) are likely to result in intense starbursts due to large tidal forces while minor mergers (galaxies with significant differences in masses) can only lead to a weak enhancement (e.g Cox et al. 2008) as the tidal perturbation with respect to the massive galaxy would be weak.

Chapter 5

SUMMARY AND CONCLUSIONS

In summary, this work aims at addressing the physics of star formation in the case of repeated interactions in a compact galaxy group by considering Stephan's Quintet and a few general compact galaxy groups as examples. The parameter space: eccentricity, galaxy spin and the pericenter passage in specific are tuned to reproduce the morphology of the Quintet to approximately match the observations. However, complexity in reproducing all the observed features through limited scope of explorable parameter space and the requirement of a more compact configuration motivated to model the general compact galaxy groups in addition to the Quintet, but at a higher resolution and incorporating the physics of star formation and feedback. The main summary and conclusions of the work presented above is as follows:

- With remarkable features from present and past interactions such as tidal tails, starburst locations and shockwave, Stephan's Quintet is a promising specimen to explore the physics of a compact galaxy group. Taking into account the recent observations, kinematics and the ages of stellar clusters in tidal features, the proposed model is able to reproduce the following features reasonably well (in the order of the interaction times): diffuse halo (from the new observations), outer tail, inner tail, tidal tail arm emanating from 7318a, relative projected positions of the members, while gas related features (main shock wave and mismatch in HI locations) and the crossed tidal tail arm from 7318b still remain irreproducible. Moreover, since the model currently does not account for a star formation model, reproducing the starburst features of the group remains a future work.

- To gain better control over the parameter space, I model repeated interactions in a three membered compact galaxy group that is spatially and temporally more compact than the Quintet. During the course of interactions, I notice the evolution of the gas density probability distribution functions compressing a large fraction of the gas into high densities. An enhancement in the SFR from ~ 5 $M_\odot/yr$ prior to the interaction to ~ 500 $M_\odot/yr$ after the first pericenter passage is noted. This enhancement is further augmented to ~ 600 $M_\odot/yr$ post second pericenter passage (Fig 3.15).

- Locations of the star formation were found to be more spatially extended prior to the starbursts, and it becomes more centrally concentrated as the interaction progresses stripping off a part of the dense gas as tidal tails and drives the rest to flow towards the nucleus (see Fig 3.17). This effect is prominent in prograde configuration due to truncation of galaxy disc but less severe in the other configurations due to comparatively weaker interactions.

- Interactions are also found to induce high velocity dispersions in the gas and these dispersions compress gas to high densities which is reflected as widened density probability distribution function. The velocity dispersion boosts approximately by an order of magnitude at the highest SFR with respect to the dispersion before the interaction and this increase in velocity dispersion is observed to cause the enhancement in SFR (Fig 3.20).

- Decomposing the repeated interactions into individual contributions, I observe that the effect of the second interaction not only drives an early onset of the SFR peaks, but also boosts the enhancement in SFR resulting from the first interaction.
- Different orbital configurations of retrograde encounter, increased pericenter passage and inclined orbit have been explored and they are found to yield a boost in the starburst. All these configurations reach the starburst regime in the Kennicutt-Schmidt plot during the interactions and reinforce interaction-driven nuclear gas inflows and enhanced velocity dispersions triggering these starburts (Fig 3.27).
- The starburst galaxies continue to form stars efficiently (i.e with short depletion time) despite their SFRs resuming almost the pre-interaction values. I have identified that high velocity dispersion in the post interaction phase to be a possible tracer of this effect, although its physical origin remains uncertain. This enhancement in velocity dispersion is atleast partly contributed by gas inflows into the galaxy.

In conclusion, although Stephan's Quintet's remarkable features make it a widely studied example in understanding the physics in repeated galaxy interactions, complexity in reproducing all the features and restricted exploration of parameter space called for modeling a general compact group. Although I note that interactions drive the galaxies to form stars very efficiently, disentangling the contributions from individual physical drivers is complex with velocity dispersion and gas inflows being two notable contributors. However, none of the discussed general compact galaxy group configurations result in a quenching or a saturation scenario of starbursts (Fig 3.25). So, the boost in starburst is more likely to occur in repeated interactions as I find this in all our configurations without aiming for it. However, this doesn't necessarily mean that the other two scenarios are not possible. Different model parameters of galaxies (e.g gas fraction, masses, types) and/or physics of star formation (e.g AGN) can possibly lead to quenching or saturation.

Appendix A

Model and orbital parameters

General compact galaxy group's model and orbital parameters. The galaxies involved are two spirals (main and the first interaction) and an elliptical (second interaction). The system is assumed to be at low redshift and hence the gas fraction in the galaxies is assumed to be 10%

Profiles	Parameters	Main	Spiral	Elliptical
Bulge	Mass ($M_\odot$)	10^{11}	$0.7 * 10^{11}$	$2.5 * 10^{11}$
	# particles	3,00,000	2,12,000	7,50,000
	scale radius (kpc)	3	1	2
	cutoff radius (kpc)	30	10	20
	scale height (kpc)	–	–	–
	cutoff height (kpc)	–	–	–
Dark Matter	Mass ($M_\odot$)	$20 * 10^{11}$	$8.8 * 10^{11}$	$13.5 * 10^{11}$
	# particles	4,00,000	1,76,000	2,70,000
	scale radius (kpc)	15	10	6
	cutoff radius (kpc)	100	60	40
	scale height (kpc)	–	–	–
	cutoff height (kpc)	–	–	–
Stellar disc	Mass ($M_\odot$)	$3 * 10^{11}$	$1.1 * 10^{11}$	–
	# particles	2,00,000	73,500	–
	scale radius (kpc)	5	3	–
	cutoff radius (kpc)	50	30	–
	scale height (kpc)	0.3	0.1	–
	cutoff height (kpc)	3	1	–
Gas disc	Mass ($M_\odot$)	$4.5 * 10^{10}$	$2 * 10^{10}$	$5 * 10^{9}$
	# particles	1,50,000	67,000	16,000
	scale radius (kpc)	6	4	1
	cutoff radius (kpc)	30	20	10
	scale height (kpc)	0.15	0.05	0.1
	cutoff height (kpc)	1.5	0.5	1
Prograde	(x, y, z) (kpc)	(0, 0, 0)	(-60, 105, 0)	(150, -80, 0)
	(v_x, v_y, v_z) (km/s)	(0, 0, 0)	(100, -470, 0)	(-450, 400, 0)
	(spin-x, spin-y, spin-z)	(0, 0, 1)	(0.5, 0.5, -0.5)	(0, 0, 1)
Retrograde	(x, y, z) (kpc)	(0, 0, 0)	(-60, 105, 0)	(150, -80, 0)
	(v_x, v_y, v_z) (km/s)	(0, 0, 0)	(100, -470, 0)	(-450, 400, 0)
	(spin-x, spin-y, spin-z)	(0, 0, -1)	(0.5, 0.5, -0.5)	(0, 0, 1)
Increased pericenter	(x, y, z) (kpc)	(0, 0, 0)	(-70, 110, 0)	(160, -50, 0)
	(v_x, v_y, v_z) (km/s)	(0, 0, 0)	(96, -451, 0)	(-451, 402, 0)
	(spin-x, spin-y, spin-z)	(0, 0, 1)	(0.5, 0.5, -0.5)	(0, 0, 1)
Inclined	(x, y, z) (kpc)	(0, 0, 0)	(-65, 110, 70)	(150, -63, -100)
	(v_x, v_y, v_z) (km/s)	(0, 0, 0)	(80, -372, -208)	(-352, 313, 290)
	(spin-x, spin-y, spin-z)	(0, 0, 1)	(0.5, 0.5, -0.5)	(0, 0, 1)

Model and orbital parameters of galaxies in Stephan's Quintet. The galaxies involved are four spirals (7319, 7320c, 7318a & 7318b) and an elliptical (7317). The system is at low redshift and hence the gas fraction in the galaxies is assumed to be 10%

Profiles	Parameters	7319	7317	7320c	7318a	7318b
Bulge	Mass ($M_\odot$)	10^{11}	$25 * 10^{10}$	$0.7 * 10^{11}$	$0.9 * 10^{11}$	$0.9 * 10^{11}$
	# particles	3,00,000	7,50,000	2,12,000	2,73,000	2,73,000
	scale radius (kpc)	3	6	1	3.5	3
	cutoff radius (kpc)	30	40	10	35	30
	scale height (kpc)	–	–	–	–	–
	cutoff height (kpc)	–	–	–	–	–
Dark Matter	Mass ($M_\odot$)	$20 * 10^{11}$	$13.5 * 10^{11}$	$8.8 * 10^{11}$	$16 * 10^{11}$	$16 * 10^{11}$
	# particles	4,00,000	2,70,000	1,76,000	3,20,000	3,20,000
	scale radius (kpc)	15	13	10	14	14
	cutoff radius (kpc)	100	80	60	85	85
	scale height (kpc)	–	–	–	–	–
	cutoff height (kpc)	–	–	–	–	–
Stellar disc	Mass ($M_\odot$)	$3 * 10^{11}$	–	$1.1 * 10^{11}$	$2.4 * 10^{11}$	$2.4 * 10^{11}$
	# particles	2,00,000	–	73,500	1,60,000	1,60,000
	scale radius (kpc)	5	–	3	4.5	4.5
	cutoff radius (kpc)	50	–	30	45	45
	scale height (kpc)	0.3	–	0.1	0.35	0.3
	cutoff height (kpc)	3	–	1	3.5	3
Gas disc	Mass ($M_\odot$)	$4.5 * 10^{10}$	$5 * 10^{9}$	$2 * 10^{10}$	$3.7 * 10^{10}$	$3.7 * 10^{10}$
	# particles	1,50,000	16,000	67,000	1,23,000	1,23,000
	scale radius (kpc)	6	4	2	3	3
	cutoff radius (kpc)	30	30	20	30	30
	scale height (kpc)	0.15	0.01	0.05	0.175	0.15
	cutoff height (kpc)	1.5	0.1	0.5	1.75	1.5
	(x, y, z) (kpc)	(-100, -100, 0)	(-288, -0.3, 0)	(170, -296, 0)	(-370, 200, -200)	(240, -100, -900)
	(v_x, v_y, v_z) (km/s)	(0, 0, 0)	(768, -112, 0)	(-391, 452, 0)	(408, -235, 210)	(-60, 0, 900)
	(spin-x, spin-y, spin-z)	(0, 0, 1)	(0, 0, 0.5)	(0, 0, -0.25)	(-0.5, 0, -0.5)	(0.5, 0, -0.5)

Bibliography

Agertz, O. et al. (2013). "Toward a Complete Accounting of Energy and Momentum from Stellar Feedback in Galaxy Formation Simulations". In: *ApJ* 770, 25, p. 25.

Agertz, Oscar et al. (2009). "Large-scale galactic turbulence: can self-gravity drive the observed HI velocity dispersions?" In: *MNRAS* 392, pp. 294–308.

Alatalo, K. et al. (2015). "Star Formation Suppression in Compact Group Galaxies: A New Path to Quenching?" In: *ApJ* 812, 117, p. 117.

Balsara, Dinshaw S. and Jongsoo Kim (2005). "Amplification of Interstellar Magnetic Fields and Turbulent Mixing by Supernova-driven Turbulence. II. The Role of Dynamical Chaos". In: *ApJ* 634, pp. 390–406.

Barnes, J. E. and L. Hernquist (1992). "Formation of dwarf galaxies in tidal tails". In: *NATURE* 360, pp. 715–717.

Bekki, K. (1995). "Gas dynamics of the central 1 KPC in galaxy mergers". In: *MNRAS* 276, pp. 9–19.

Bennett, C. L. et al. (2013). "Nine-year Wilkinson Microwave Anisotropy Probe (WMAP) Observations: Final Maps and Results". In: *ApJs* 208, 20, p. 20.

Berger, M. J. and P. Colella (1989). "Local adaptive mesh refinement for shock hydrodynamics". In: *Journal of Computational Physics* 82, pp. 64–84.

Bergvall, N., E. Laurikainen, and S. Aalto (2003). "Galaxy interactions - poor starburst triggers. III. A study of a complete sample of interacting galaxies". In: *AAP* 405, pp. 31–52.

Berkhuijsen, E. M. and A. Fletcher (2008). "Density probability distribution functions of diffuse gas in the Milky Way". In: *MNRAS* 390, pp. L19–L23.

Bigiel, F. et al. (2008). "The Star Formation Law in Nearby Galaxies on Sub-Kpc Scales". In: *AJ* 136, pp. 2846–2871.

Bondi, H. (1952). "On spherically symmetrical accretion". In: *MNRAS* 112, p. 195.

Bournaud, Frédéric et al. (2010). "ISM properties in hydrodynamic galaxy simulations: turbulence cascades, cloud formation, role of gravity and feedback". In: *Monthly Notices of the Royal Astronomical Society* 409.3, pp. 1088–1099.

Burbidge, E. M., G. R. Burbidge, and F. Hoyle (1963). "Condensations in the Intergalactic Medium." In: *ApJ* 138, p. 873.

Casasola, V., D. Bettoni, and G. Galletta (2004). "The gas content of peculiar galaxies: Strongly interacting systems". In: *AAP* 422, pp. 941–950.

Chabrier, Gilles (2003). "Galactic Stellar and Substellar Initial Mass Function". In: *Publications of the Astronomical Society of the Pacific* 115, pp. 763–795.

Cluver, M. E. et al. (2010). "Powerful H_2 Line Cooling in Stephan's Quintet. I. Mapping the Significant Cooling Pathways in Group-wide Shocks". In: 710, pp. 248–264.

Combes, F. et al. (1994). "CO in paired galaxies: Star formation induced by gas flow". In: *AAP* 281, pp. 725–736.

Courty, S. and J. M. Alimi (2004). "Thermodynamic evolution of cosmological baryonic gas. I. Influence of non-equipartition processes". In: *AAP* 416, pp. 875–888.

Cox, T. J. et al. (2008). "The effect of galaxy mass ratio on merger-driven starbursts". In: *MNRAS* 384, pp. 386–409.

Daddi, E. et al. (2010a). "Different Star Formation Laws for Disks Versus Starbursts at Low and High Redshifts". In: *ApJl* 714, pp. L118–L122.

Daddi, E. et al. (2010b). "Very High Gas Fractions and Extended Gas Reservoirs in z = 1.5 Disk Galaxies". In: *ApJ* 713, pp. 686–707.

Delgado-Donate, E. J. et al. (2003). "Dwarfs after mergers? The case of NGC 520, NGC 772, Arp 141, NGC 3226/7, NGC 3656 and Arp 299". In: *AAP* 402, pp. 921–928.

Di Matteo, P. et al. (2007). "Star formation efficiency in galaxy interactions and mergers: a statistical study". In: *AAP* 468, pp. 61–81.

Di Matteo, P. et al. (2008). "On the frequency, intensity, and duration of starburst episodes triggered by galaxy interactions and mergers". In: *AAP* 492, pp. 31–49.

Di Matteo, Tiziana, Volker Springel, and Lars Hernquist (2005). "Energy input from quasars regulates the growth and activity of black holes and their host galaxies". In: *NAT* 433, pp. 604–607.

Dressler, A. (1980). "Galaxy morphology in rich clusters - Implications for the formation and evolution of galaxies". In: *ApJ* 236, pp. 351–365.

Dubois, Yohan et al. (2013a). "AGN-driven quenching of star formation: morphological and dynamical implications for early-type galaxies". In: *MNRAS* 433, pp. 3297–3313.

Dubois, Yohan et al. (2013b). "Blowing cold flows away: the impact of early AGN activity on the formation of a brightest cluster galaxy progenitor". In: *MNRAS* 428, pp. 2885–2900.

Duc, P.-A. and I. F. Mirabel (1994). "Recycled galaxies in the colliding system ARP 105". In: *AAP* 289, pp. 83–93.

Duc, P.-A. and F. Renaud (2013). "Tides in Colliding Galaxies". In: *Lecture Notes in Physics, Berlin Springer Verlag*. Ed. by J. Souchay, S. Mathis, and T. Tokieda. Vol. 861. Lecture Notes in Physics, Berlin Springer Verlag, p. 327.

Duc, P.-A., J.-C. Cuillandre, and F. Renaud (2018). "Revisiting Stephan's Quintet with deep optical images". In: *mnras* 475, pp. L40–L44.

Eddington, A. S. (1916). "The distribution of stars in globular clusters". In: *MNRAS* 76, pp. 572–585.

Efstathiou, G. (2000). "A model of supernova feedback in galaxy formation". In: *MNRAS* 317, pp. 697–719.

Elmegreen, B. G. (1994). "Starbursts by gravitational collapse in the inner Lindblad resonance rings of galaxies". In: *ApJl* 425, pp. L73–L76.

Evans II, N. J. et al. (2009). "The Spitzer c2d Legacy Results: Star-Formation Rates and Efficiencies; Evolution and Lifetimes". In: *Apjs* 181, pp. 321–350.

Evans II, N. J., A. Heiderman, and N. Vutisalchavakul (2014). "Star Formation Relations in Nearby Molecular Clouds". In: *ApJ* 782, 114, p. 114.

Fedotov, K. et al. (2011). "Star Clusters as Tracers of Interactions in Stephan's Quintet (Hickson Compact Group 92)". In: *AJ* 142, 42, p. 42.

Fensch, J. et al. (2017). "High-redshift major mergers weakly enhance star formation". In: *MNRAS* 465, pp. 1934–1949.

Focardi, P. and B. Kelm (2002). "Compact groups in the UZC galaxy sample". In: *AAP* 391, pp. 35–46.

Georgakakis, A., D. A. Forbes, and R. P. Norris (2000). "Cold gas and star formation in a merging galaxy sequence". In: *MNRAS* 318, pp. 124–138.

Gerhard, O. E. (1981). "N-body simulations of disc-halo galaxies - Isolated systems, tidal interactions and merging". In: *MNRAS* 197, pp. 179–208.

Gnedin, N. Y., E. J. Tasker, and Y. Fujimoto (2014). "Emergence of the Kennicutt-Schmidt Relation from the Small-scale SFR-Density Relation". In: *APJl* 787, L7, p. L7.

Gunn, J. E. and J. R. Gott III (1972). "On the Infall of Matter Into Clusters of Galaxies and Some Effects on Their Evolution". In: *ApJ* 176, p. 1.

Haardt, F. and P. Madau (1996). "Radiative Transfer in a Clumpy Universe. II. The Ultraviolet Extragalactic Background". In: *ApJ* 461, p. 20.

Hernquist, L. (1990). "An analytical model for spherical galaxies and bulges". In: *ApJ* 356, pp. 359–364.

Hickson, P. (1982). "Systematic properties of compact groups of galaxies". In: *ApJ* 255, pp. 382–391.

Hwang, J.-S. et al. (2012). "Models of Stephan's Quintet: hydrodynamic constraints on the group's evolution". In: *MNRAS* 419, pp. 1780–1794.

Hwang, Jeong-sun (2010). "Models of galaxy collisions in Stephan's Quintet and other interacting systems". In: *Graduate Theses and Dissertations* 11288.

Iovino, A. et al. (2003). "A New Sample of Distant Compact Groups from the Digitized Second Palomar Observatory Sky Survey". In: *AJ* 125, pp. 1660–1681.

Ishibashi, W. and A. C. Fabian (2012). "Active galactic nucleus feedback and triggering of star formation in galaxies". In: *MNRAS* 427, pp. 2998–3005.

Jog, Chanda J. and P. M. Solomon (1992). "A Triggering Mechanism for Enhanced Star Formation in Colliding Galaxies". In: *ApJ* 387, p. 152.

Jogee, S. et al. (2008). "Frequency and Impact of Galaxy Mergers and Interactions over the Last 7 Gyr". In: *Formation and Evolution of Galaxy Disks*. Ed. by J. G. Funes and E. M. Corsini. Vol. 396. Astronomical Society of the Pacific Conference Series, p. 337.

Jubelgas, M. et al. (2008). "Cosmic ray feedback in hydrodynamical simulations of galaxy formation". In: *AAP* 481, pp. 33–63.

Karachentseva, V. E. and I. D. Karachentsev (2000). "Southern triplets of galaxies". In: *IAU Colloq. 174: Small Galaxy Groups*. Ed. by M. J. Valtonen and C. Flynn. Vol. 209. Astronomical Society of the Pacific Conference Series, p. 11.

Kawata, D. and J. S. Mulchaey (2008). "Strangulation in Galaxy Groups". In: *ApJl* 672, p. L103.

Kennicutt Jr., R. C. (1998a). "The Global Schmidt Law in Star-forming Galaxies". In: *ApJ* 498, pp. 541–552.

— (1998b). "The Global Schmidt Law in Star-forming Galaxies". In: *ApJ* 498, pp. 541–552.

Kennicutt Jr., R. C. et al. (2007). "Star Formation in NGC 5194 (M51a). II. The Spatially Resolved Star Formation Law". In: *ApJ* 671, pp. 333–348.

Kravtsov, A. V. (2003). "On the Origin of the Global Schmidt Law of Star Formation". In: *ApJl* 590, pp. L1–L4.

Krumholz, M. R. and T. A. Thompson (2007). "The Relationship between Molecular Gas Tracers and Kennicutt-Schmidt Laws". In: *ApJ* 669, pp. 289–298.

Krumholz, M. R., C. F. McKee, and J. Tumlinson (2009a). "The Atomic-to-Molecular Transition in Galaxies. II: H I and H_2 Column Densities". In: *ApJ* 693, pp. 216–235.

— (2009b). "The Star Formation Law in Atomic and Molecular Gas". In: *ApJ* 699, pp. 850–856.

Larson, R. B. and B. M. Tinsley (1978). "Star formation rates in normal and peculiar galaxies". In: *ApJ* 219, pp. 46–59.

Lauberts, A. (1974). "Encounters between Galaxies of Equal Size". In: *AAP* 33, p. 231.

Mac Low, M.-M. and R. S. Klessen (2004). "Control of star formation by supersonic turbulence". In: *Reviews of Modern Physics* 76, pp. 125–194.

Martig, M. et al. (2009). "Morphological Quenching of Star Formation: Making Early-Type Galaxies Red". In: *ApJ* 707, pp. 250–267.

Michiyama, T. et al. (2016). "Investigating the relation between CO (3-2) and far-infrared luminosities for nearby merging galaxies using ASTE". In: *PASJ* 68, 96, p. 96.

Mihos, J. C. and L. Hernquist (1996). "Gasdynamics and Starbursts in Major Mergers". In: *ApJ* 464, p. 641.

Mihos, J. C., D. O. Richstone, and G. D. Bothun (1991). "A numerical study of star formation in interacting disk galaxies". In: *ApJ* 377, pp. 72–88.

Miki, Y. and M. Umemura (2017). "MAGI: many-component galaxy initialiser". In: *ArXiv e-prints*.

Molina, F. Z. et al. (2012). "The Density Variance–Mach Number Relation in Supersonic Turbulence: I. Isothermal, magnetised gas". In: *arXiv e-prints*, arXiv:1203.2117, arXiv:1203.2117.

Moore, B. et al. (1996). "Galaxy harassment and the evolution of clusters of galaxies". In: *Nature* 379, pp. 613–616.

Murray, N. (2011). "Star Formation Efficiencies and Lifetimes of Giant Molecular Clouds in the Milky Way". In: *ApJ* 729, 133, p. 133.

Navarro, J. F., C. S. Frenk, and S. D. M. White (1996). "The Structure of Cold Dark Matter Halos". In: *ApJ* 462, p. 563.

Noguchi, M. and S. Ishibashi (1986). "Simulations of close encounter between galaxies - Behaviour of interstellar gas clouds and enhancement of star formation rate". In: *MNRAS* 219, pp. 305–331.

Oliva-Altamirano, P. et al. (2018). "The connection between the peaks in velocity dispersion and star-forming clumps of turbulent galaxies". In: *MNRAS* 474, pp. 522–535.

Ostriker, J. P. and C. F. McKee (1988). "Astrophysical blastwaves". In: *Reviews of Modern Physics* 60, pp. 1–68.

O'Sullivan, E. et al. (2009). "A Chandra X-ray View of Stephan's Quintet: Shocks and Star Formation". In: *ApJ* 701, pp. 1560–1568.

Pan, Hsi-An et al. (2018). "The Effect of Galaxy Interactions on Molecular Gas Properties". In: *ArXiv e-prints*, arXiv:1810.10162, arXiv:1810.10162.

Perret, V. et al. (2014). "Evolution of the mass, size, and star formation rate in high redshift merging galaxies. MIRAGE - A new sample of simulations with detailed stellar feedback". In: *AAP* 562, A1, A1.

Ponman J., T et al. (1994). "A possible fossil galaxy group". In: *NATURE* 369, pp. 462–464.

Pontzen, A. et al. (2017). "How to quench a galaxy". In: *MNRAS* 465, pp. 547–558.

Powell, Leila C. et al. (2013). "Beyond the nuclear starburst? Clustered star formation in major mergers". In: *MNRAS* 434, pp. 1028–1042.

Raiteri, C. M., M. Villata, and J. F. Navarro (1996). "Simulations of Galactic chemical evolution. I. O and Fe abundances in a simple collapse model." In: *AAP* 315, pp. 105–115.

Rasmussen, J. et al. (2008). "Galaxy evolution in Hickson compact groups: the role of ram-pressure stripping and strangulation". In: *MNRAS* 388, pp. 1245–1264.

Renaud, F., C. Theis, and C. M. Boily (2008). "Starburst triggered by compressive tides in galaxy mergers". In: *Astronomische Nachrichten* 329, p. 1050.

Renaud, F., P. N. Appleton, and C. K. Xu (2010). "N-body Simulation of the Stephan's Quintet". In: *ApJ* 724, pp. 80–91.

Renaud, F. et al. (2014). "Starbursts triggered by intergalactic tides andinterstellar compressive turbulence". In: *MNRAS* 442, pp. L33–L37.

Renaud, Florent et al. (2019). "A diversity of starburst-triggering mechanisms in interacting galaxies and their signatures in CO emission". In: *arXiv e-prints*, arXiv:1902.02353, arXiv:1902.02353.

Rose, J. A. (1977). "A survey of compact groups of galaxies." In: *ApJ* 211, pp. 311–318.

Sanders, D. B. and I. F. Mirabel (1985). "CO detections and IRAS observations of bright radio spiral galaxies at CZ equal or less than 9000 kilometers per second". In: *ApJl* 298, pp. L31–L35.

Sanduleak, N. (1969). "Correlation of the Distributions of Young Stars and Neutral Hydrogen in the Small Magellanic Cloud". In: *AJ* 74, p. 47.

Schmidt, M. (1959). "The Rate of Star Formation." In: *ApJ* 129, p. 243.

Shu, F. H., F. C. Adams, and S. Lizano (1987). "Star formation in molecular clouds - Observation and theory". In: *ARAA* 25, pp. 23–81.

Sijacki, Debora et al. (2007). "A unified model for AGN feedback in cosmological simulations of structure formation". In: *MNRAS* 380, pp. 877–900.

Silk, J. and M. J. Rees (1998). "Quasars and galaxy formation". In: *AAP* 331, pp. L1–L4.

Sofue, Y. et al. (1993). "CO observations of Arp's interacting galaxies". In: *PASJ* 45, pp. 43–55.

Solomon, P. M. and L. J. Sage (1988). "Star-formation rates, molecular clouds, and the origin of the far-infrared luminosity of isolated and interacting galaxies". In: *ApJ* 334, pp. 613–625.

Sulentic, J. W. (2002). "Compact Galaxy Groups in 3D (Invited Talk)". In: *Galaxies: the Third Dimension*. Ed. by M. Rosada, L. Binette, and L. Arias. Vol. 282. Astronomical Society of the Pacific Conference Series, p. 227.

Tabatabaei, F. S. et al. (2013). "Multi-scale radio-infrared correlations in M 31 and M 33: The role of magnetic fields and star formation". In: *AAP* 557, A129, A129.

Tchekhovskoy, Alexander and Jonathan C. McKinney (2012). "Prograde and retrograde black holes: whose jet is more powerful?" In: *MNRAS* 423, pp. L55–L59.

Telesco, C. M. et al. (1984). "A luminous 3 kiloparsec infrared disk in NGC 1068". In: *ApJ* 282, pp. 427–435.

Teyssier, R. (2002). "Cosmological hydrodynamics with adaptive mesh refinement. A new high resolution code called RAMSES". In: *A&A* 385, pp. 337–364.

Teyssier, R., D. Chapon, and F. Bournaud (2010). "The Driving Mechanism of Starbursts in Galaxy Mergers". In: *ApJl* 720, pp. L149–L154.

Toomre, A. and J. Toomre (1972). "Galactic Bridges and Tails". In: *ApJ* 178, pp. 623–666.

Tully, R. B. (1987). "Nearby groups of galaxies. II - an all-sky survey within 3000 kilometers per second". In: *ApJ* 321, pp. 280–304.

Tzanavaris, P. et al. (2010). "Hickson Compact Groups with Swift and Spitzer". In: *9th International Conference of the Hellenic Astronomical Society*. Ed. by K. Tsinganos, D. Hatzidimitriou, and T. Matsakos. Vol. 424. Astronomical Society of the Pacific Conference Series, p. 316.

Van Loo, Sven, Jonathan C. Tan, and Sam A. E. G. Falle (2015). "Magnetic Fields and Galactic Star Formation Rates". In: *ApJ* 800, L11, p. L11.

Vazquez-Semadeni, E. (1994). "Hierarchical Structure in Nearly Pressureless Flows as a Consequence of Self-similar Statistics". In: *ApJ* 423, p. 681.

Vorontsov-Velyaminov, B. (1962). "Interaction of Multiple Systems". In: *Problems of Extra-Galactic Research*. Ed. by G. C. McVittie. Vol. 15. IAU Symposium, p. 194.

Wang, P. and T. Abel (2009). "Magnetohydrodynamic Simulations of Disk Galaxy Formation: The Magnetization of the Cold and Warm Medium". In: *ApJ* 696, pp. 96–109.

Wang, Z. et al. (2004). "The Off-Nuclear Starbursts in NGC 4038/4039 (The Antennae Galaxies)". In: *ApJs* 154, pp. 193–198.

White, S. D. M. and M. J. Rees (1978). "Core condensation in heavy halos - A two-stage theory for galaxy formation and clustering". In: *MNRAS* 183, pp. 341–358.

Whitmore, B. C. et al. (1999). "The Luminosity Function of Young Star Clusters in "the Antennae" Galaxies (NGC 4038-4039)". In: *AJ* 118, pp. 1551–1576.

Williams, B. A., M. S. Yun, and L. Verdes-Montenegro (2002). "The VLA H I Observations of Stephan's Quintet (HCG 92)". In: *AJ* 123, pp. 2417–2437.

Xu, C. K. et al. (2005). "Ultraviolet Emission and Star Formation in Stephan's Quintet". In: *ApJl* 619, pp. L95–L98.

Zwicky, F. (1956). "Multiple Galaxies". In: *Ergebnisse der exakten Naturwissenschaften* 29, pp. 344–385.

— (1962). "Supernovae and Chains of Supernovae as Launchers of Stars and Galaxies". In: *PASP* 74, p. 70.